Delamination buckling and postbuckling in composite cylindrical shells under combined axial compression and external pressure

DOI:
10.1016/j.compstruct.2005.01.009

Tafreshi, A. Apr 2006 In : Composite Structures. 72, 4, p. 401-418 17 p.

DELAMINATION BUCKLING AND POSTBUCKLING IN COMPOSITE CYLINDRICAL SHELLS UNDER COMBINED AXIAL COMPRESSION AND EXTERNAL PRESSURE

Azam Tafreshi Aerospace Engineering
School of Mechanical, Aerospace and Civil Engineering (MACE)
University of Manchester, Oxford Road,
Manchester M13 9PL, UK, atafreshi@man.ac.uk

Abstract

Keywords: Delamination, composites, finite element method, buckling analysis, laminated cylindrical shells, external pressure, axial compression, postbuckling

A series of finite element analyses on the delaminated composite cylindrical shells subject to combined axial compression and pressure are carried out varying the delamination thickness and length, material properties and stacking sequence. Based on the FE results, the characteristics of the buckling and postbuckling behaviour of delaminated composite cylindrical shells are investigated. The combined double-layer and single-layer of shell elements are employed which in comparison with the three-dimensional finite elements requires less computing time and space for the same level of accuracy. The effect of contact in the buckling mode has been considered, by employing contact elements between the delaminated layers. The interactive buckling curves and postbuckling response of delaminated cylindrical shells have been obtained. In the analysis of post-buckled delaminations, a study using the virtual crack closure technique has been performed to find the distribution of the local strain energy release rate along the delamination front. The results are compared with the previous results obtained by the author on the buckling and postbuckling of delaminated composite cylindrical shells under the axial compression and external pressure, applied individually.

Nomenclature

a	Length of delamination
$\bar{a}$ =a/L	Normalized delamination length
E_{11}, E_{22}, G_{12}, ν_{12}	Material constants
G	Strain energy release rate
t_1, t_2	Thicknesses of upper and lower sublaminates, respectively
$h=t_1/t$	Normalized delamination thickness
L,r,t	Length, radius and thickness of the overall cylindrical shell, respectively
X,Y,Z	Nodal force components in the x,y and z directions, respectively
P	Pressure
P_c	Critical buckling pressure of an intact cylinder under external pressure alone
P_{cr}	Critical buckling pressure of a delaminated cylinder
R	Compressive axial load
R_c	Critical axial compression of an intact cylinder under axial compressive alone
R_{cr}	Critical axial compression of a delaminated cylinder
u(or u_x),v(or u_y),w(or u_z)	Axial, circumferential and radial displacements, respectively
x,y,z	Axial, circumferential and radial coordinates, respectively
α	Angle of the delamination region
ψ_x, ψ_y, ψ_z	Rotation about the y, x, and z axes, respectively

1. INTRODUCTION

Laminated composite materials are increasingly being used in the aerospace, marine, automobile and other engineering industries. This is due to their high strength and stiffness-to-weight ratios. However, due to the lack of through-the-thickness reinforcement, structures made from these materials are highly liable to failures caused by

delamination. Therefore, within a design process, a structure's resistance to delamination should be addressed to maximize its durability and damage tolerance.

The phenomenon of progressive failure in laminated composite structures is yet to be understood, and as a result, reliable strategies for designing optimal composite structures for desired life and strength are in demand [1-2].

Delaminations in composite cylinders may be due to manufacturing defects, transportation impacts and environmental effects during their service life. The presence of delaminations leads to a reduction in the overall buckling strength of the structure [3-4]. For the past two decades analytical and numerical analyses have been carried out by many researchers to analyse delaminated composite structures, considering their buckling and post-buckling behaviour[5-6]. Almost all of the papers on delamination buckling deal with beams and flat plates.[7-16]. The early work belongs to Chai et al.[9] who characterized the delamination buckling models by the delamination thickness and the number of delaminations through the laminate thickness.

There are many publications available on the buckling and post-buckling analysis of perfect and imperfect cylindrical shells and panels subject to axial compression, external pressure, bending, etc.[17-23]. Due to its mathematical complexity and modelling, very limited information on the subject of delamination buckling of cylindrical shells and panels is currently available [3-4, 24-33]. The most comprehensive analytical study is by Simitses et al[25-27]. Simitses et al [25-27] analytically predicted delamination buckling of cylindrical shells and panels. The load cases considered in their study were uniform axial compression and uniform external pressure, applied individually. For both cases they did not account for the contact between delaminated layers during buckling.

In the recent numerical studies [3-4] by the author, delamination buckling and postbuckling of composite cylindrical shells under axial compression [3] and external pressure [4], applied individually, were considered. For both loading cases, the effect of contact between the delaminated layers was taken into account. The use of three-dimensional

finite elements for the modelling of delamination in cylindrical shells is computationally expensive. Therefore, an efficient modelling approach was employed for the investigation of the buckling and postbuckling behaviour of these structures. In each case the results were compared with the corresponding results obtained by Simitses et al [25-27]. It is shown that ignoring the contact between the delaminated layers could result in wrong estimations of the critical buckling loads in cylindrical shells under axial compression or external pressure.

There is a reasonable amount of work on the buckling and postbuckling of laminated cylindrical shells under combined loading [34-41]. Despite the relatively widespread attention given to the problem of delamination in laminated composites, to the author's knowledge, there is no information available on the effect of delamination in a composite cylindrical shell structure under combined loading.

This paper deals with the computational modelling of delamination buckling and postbuckling of laminated composite cylindrical shells subjected to combined axial compression and external pressure. Some results are also provided on the influence of internal pressure on buckling under the action of axial compression. Some parametric studies are performed to investigate the influence of the delamination size and through-the-thickness position on the critical loads of a series of delaminated cylindrical shells. The effects of the material properties and stacking sequence of laminated cylindrical shells are also investigated. Using the virtual crack closure technique (VCCT), variation of the strain energy release rate(SERR) along the delamination front is determined[42-43].

The analysis has been carried out using ABAQUS 6.4[44], which is available on the mainframe computer, Bezier, at Manchester Computing Centre.

2. BUCKLING AND POSTBUCKLING ANALYSIS USING THE FINITE ELEMENT METHOD

The three-dimensional finite elements can model the delamination behaviour of laminates very well but they are computationally expensive. In order to reduce the computational time and capacity for the same level of accuracy, the alternative is to employ a combined double-layer and single-layer of shell elements. The following explains the FE modelling, buckling and postbuckling procedures and also the method employed for calculation of the strain energy release rate (SERR) in this study, respectively. This is a similar procedure employed by the author in references [3-4], where the buckling and postbuckling analyses of laminated cylindrical shells were performed. The load cases considered in those references were uniform axial compression [3] and external pressure [4], applied individually.

Fig.1i-a shows the geometry of a typical cylindrical shell with a delamination width of *a* extended along its entire circumference. The delamination is located symmetrically with respect to both ends of the shell. r and L are the radius and length of the cylinder, while t_1 and t_2 are the thicknesses of the upper and lower sublaminates, respectively. The nondimensional parameter $h=t_1/t$ is used to describe the delamination thickness, where t is the thickness of the cylinder. The cylinder is clamped at both ends and is subjected to simultaneous loading of axial compression, R, and lateral pressure, P.

Fig. 1-ib shows a differential element of an intact cylindrical shell segment with the coordinate axes. The axial coordinate is x, the circumferential coordinate is y, and the thickness coordinate normal to the shell surface is z. The circumferential coordinate can be replaced by $y=R\beta$.

For the finite element analysis of a typical cylindrical shell, a single layer of shell elements, designated S8R in ABAQUS, can be employed and the corresponding buckling and postbuckling analysis can be performed. S8R is an eight noded shear deformable shell element with reduced integration, which allows large rotations and small strains.

The displacement field for an intact cylindrical shell, according to a first order shear deformation theory, is given by

$$\begin{aligned} u_x &= u_x^0 + z\psi_x \\ u_y &= u_y^0 + z\psi_y \\ u_z &= u_z^0 \end{aligned} \qquad (1)$$

u_x, u_y, u_z are the displacements (in the x, y and z directions, respectively) and ψ_x, ψ_y are the rotations (about y and x axes, respectively), at arbitrary locations with the distance z to the shell's mid-surface. u_x^0, u_y^0, u_z^0 are the mid-surface displacements of the shell in the respective directions.

For the computational analysis of a delaminated cylinder, the intact regions can be represented by a single-layer of shell elements, whereas the delaminated regions can be modelled by upper and lower sublaminates that are connected by contact elements, designated GAP in ABAQUS. For the interface region, a modified version of the sublaminate connection method, based on Eq.(1), must be employed. Therefore, also the rotations(ψ_x, ψ_y, ψ_z) of all the nodes of the stacked layers at the transition border are coupled in addition to the displacements(u_x, u_y, u_z). Thus, the mid-surfaces of the sublaminates of the delaminated and the mid-surface of the laminate of the intact area are coupled by the following set of equations:

$$\begin{aligned} u_x^{1,0} - \left(\frac{t_1}{2}\right)\psi_x^1 &= u_x^{2,0} + \left(\frac{t_2}{2}\right)\psi_x^2 = u_x^0 \\ u_y^{1,0} - \left(\frac{t_1}{2}\right)\psi_y^1 &= u_y^{2,0} + \left(\frac{t_2}{2}\right)\psi_y^2 = u_y^0 \\ u_z^{1,0} &= u_z^{2,0} = u_z^0 \\ \psi_x^1 &= \psi_x^2 = \psi_x^0 \\ \psi_y^1 &= \psi_y^2 = \psi_y^0 \\ \psi_z^1 &= \psi_z^2 = \psi_z^0 \end{aligned} \qquad (2)$$

The consistency and accuracy of the combined single layer and double layer of shell elements was verified in Ref.[3]. An FE analysis was performed on a simply supported

intact laminated curved panel with a stacking sequence of $[\pm\theta/\pm\theta/\theta]_s$. The buckling loads of the curved panel for various winding angles were obtained. The panel was modelled using a single layer of shell elements and also double layer of shell elements. The critical buckling loads were compared with the analytical results of Jaunky and Knight[Ref. 17], which were in very good agreement. Quadratic quadrilateral shell elements, designated S8R in ABAQUS, were employed for the modelling of each layer.

It should be noted that the proposed modelling is applicable for any shape of the delamination. In a study by the author [7], the combined single-layer and double-layer of shell elements were employed to investigate the global buckling behaviour and local damage propagation of composite flat plates containing embedded delaminations. A parametric study was carried out to investigate the influence of the delamination size, thickness, shape and alignment of a series of composite plates. Some of the results were compared with the corresponding experimental results [12], which were in good agreement.

In another study by the author [3], the above method was employed to study the effect of delamination on the global load-carrying capacity of isotropic and laminated composite cylindrical shells under axial compression. The delaminstions were either rectangular or with a constant length extended along the entire circumference of the cylinder. A parametric study was performed to study the influence of the delamination size, orientation and through-the-thickness position of a series of laminated cylinders. The effect of material properties was also investigated. Some of the results were compared with the corresponding analytical results obtained by Simitses et al [26]. An example of a cylindrical shell made of isotropic material with clamped ends under axial compression, similar to the model employed by Simitses et al[26], was presented in Ref.[3] to validate the proposed FE modelling approach. The delamination was located symmetrically with respect to both ends of the shell and it extended along its entire circumference. See Fig. 1-ii. The dimensions of the shell are such that L/r=5 and r/t=30. The numerical results of variation of critical load with delamination length and delamination thickness, obtained using the present method, were compared with those obtained by Simitses et al[26], as shown in Fig.1-ii. The critical loads are normalized with respect to the critical load of an

intact cylinder. It is shown that although Simitses et al [26] did not account for the contact, between delaminated layers during buckling, their results look reasonable. For the delamination thicknesses of h=0.3 and 0.5, with delamination length of $\bar{a}$ >0.04, the buckling load will increase when considering the effect of contact in the buckling mode. For the delamination thickness of h=0.1, with delamination length of $\bar{a}$ >0.04, the effect of contact in the buckling mode is almost negligible. This figure also shows that, for very small values of the delamination length($\bar{a}$ <0.01), regardless of the delamination thickness and also the effect of contact, the delamination has no significant effect on the critical loads. For the delamination length of (0.01< $\bar{a}$ <0.04), the buckling load will decrease when considering the effect of contact in the buckling mode.

The selection of the mid-surface as a reference surface in a shell element is due to tradition and the ease of defining bending and shear rigidities. However, for composite laminates with delaminations, it leads to the complexity of using constraint equations (Eq. 2) to maintain compatibility of displacements on the delaminated front. The other disadvantage is for use with the virtual crack closure technique (VCCT) for calculation of the strain energy release rate(SERR). The latter is explained in more detail in references [6-7]. An alternative method, which overcomes these difficulties and also simplifies the mesh generation, is to choose the reference surface at an arbitrary position within the shell's thickness. According to the first order, shear deformation theory (Eq. 1), the deformation at any position within the thickness direction can be expressed by the deformation at any chosen surface, not necessarily the shell's mid-surface.

Fig.1-ic shows the close-up view of an FE model that can overcome the problems mentioned above. This FE model is also a combination of double-layer and single-layer of shell elements; however, the delaminated surface is chosen as the reference surface for both the intact and delaminated regions. In the delaminated region, nodes are separately defined on the upper and lower sublaminates although they may have the same coordinates. Gap elements are placed between the corresponding nodes of the upper and lower sublaminates to avoid the interpenetration of the delaminated layers. Within the intact and delaminated regions, the nodes located on the reference surface are offset from the mid-surfaces of the

corresponding shells, either in the positive or negative direction. To achieve this requirement the OFFSET command [44] with shell elements is employed. To maintain compatibility of displacements on the delaminated front, the nodes of the intact and delaminated regions are tied together to have equal deformations.

The aforementioned FE model, shown in Fig. 1-ic, was employed by the author in Ref. [4] to investigate the delamination buckling and postbuckling of composite cylindrical shells under external pressure. The delaminstions were either rectangular or had a constant width extended along the entire length of the cylinder. It was shown that through-the-thickness delamination can be modelled and analysed effectively without requiring a great deal of computing time and memory. A parametric study was also carried out to investigate the influence of the delamination size, orientation and through-the-thickness position of a series of laminated cylinders. In the analysis of post-buckled delaminations, a study using virtual crack closure technique was performed to find the distribution of the local strain energy release rate along the delamination front. The effects of material properties and stacking sequence were also examined.

An example of a laminated cylindrical shell with longitudinal delamination over the entire length under external pressure, similar to the model employed by Simitses et al [26], was presented in Ref.[4]. The material used was graphite-epoxy(Table-1) and the cross-ply laminates had the stacking sequence of $[90^o/0^o/90^o]_{10T}$. The cylinder was simply supported at both ends. See Fig. 1-iii. The dimensions of the shell were such that L/r=6 and r/t=100.

The numerical results of variation of critical pressure with delamination width(α) and delamination thickness(h), calculated using the present method, were compared with those obtained by Simitses et al[26]. See Fig.1-iii. The critical loads are normalized with respect to the critical load of an intact cylinder. Figs. 1-iiia and 1-iiic show that for the delamination thicknesses of h=0.5 and 0.1 although Simitses et al [26] did not account for the contact (between delaminated layers during buckling) their results agree reasonably well with the results presented in Ref. [4]. However, Fig. 1-iiib shows that for the

delamination thickness of h=0.3 there is a large discrepancy of up to 50%, when considering the effect of contact in the buckling mode.

The significant difference between the results of Ref.[4] and those of Simitses et al[26], for the case of h=0.3, is obviously due to the material interpenetration at the delaminated layers, when the effect of contact is not considered. To investigate the effect of material interpenetration at the debonded region, the buckling curve for h=0.3 and $0.<\alpha<360°$, for the case without gap elements, was also obtained. See Fig. 1-iiib. It can be seen that this curve is reasonably close to the buckling curve of reference 26.

It was also observed that for h=0.5, the delaminated cylinder mainly buckles in a global mode, with or without having contact elements between the delaminated layers. Therefore, the effect of contact in this case is almost negligible. For h=0.3, when the contact elements are removed, the cylinder mainly buckles locally and there is serious penetration between the delaminated layers. As a result in this case, the influence of contact turns out to be high. For h=0.1, the very thin upper delaminated layer tends to buckle independently, and the critical buckling load is very low, whenever considering or ignoring the effect of contact.

In the present paper, the FE model, shown in Fig.1-ic, has also been employed for the study of delamination buckling and postbuckling of composite cylindrical shells under combined axial compression and external pressure. The first stage in the simulation is a linear eigenvalue buckling analysis. This was carried out in two steps. In the first step a live pressure load was applied to the shell, and then an axial compressive load was applied to the pressurized shell in the second step. Following the eigenvalue analysis, the postbuckling analysis has been performed. Arc length methods such as the Riks method available in ABAQUS, are global load-control methods that are suitable for global buckling and postbuckling analyses; they do not function well when buckling is localized. In the current study, the automatic stabilization in ABAQUS, which applies volume proportional damping to the structure, is used. In the dynamic case, the strain energy released locally from buckling is transformed into kinetic energy; in the damping case, the strain energy is

dissipated. It should be noted that the initial small deflection that is necessary to make the structure buckle was established by an imperfection to the upper delaminated layer. The applied imperfection rested on an eigenmode buckling analysis of the structure, similar to the method employed by the author in Refs.[3,4,7,34]. The maximum initial perturbation was 5% of the thickness of the shell.

The virtual crack closure technique (VCCT) is used to calculate the strain energy release rate(SERR). The nodal forces at the crack front and the displacements behind the crack front are used to calculate SERR [42-43]. Fig. 2 shows a model of a pair of four elements in the upper and lower sublaminates at the delamination front. The crack front is located beneath nodes c_j (j=1,5). The components of the strain energy release rate for the three modes for a typical element are

$$G_I = \frac{1}{2\Delta A}\left\{Z_{c_3}\left(w_{a_3} - w_{A_3}\right) + Z_{d_2}\left(w_{b_2} - w_{B_2}\right) + \frac{1}{2}\left[Z_{c_2}\left(w_{a_2} - w_{A_2}\right) + Z_{c_4}\left(w_{a_4} - w_{A_4}\right)\right]\right\}$$

$$G_{II} = \frac{1}{2\Delta A}\left\{X_{c_3}\left(u_{a_3} - u_{A_3}\right) + X_{d_2}\left(u_{b_2} - u_{B_2}\right) + \frac{1}{2}\left[X_{c_2}\left(u_{a_2} - u_{A_2}\right) + X_{c_4}\left(u_{a_4} - u_{A_4}\right)\right]\right\} \qquad (3)$$

$$G_{III} = \frac{1}{2\Delta A}\left\{Y_{c_3}\left(v_{a_3} - v_{A_3}\right) + Y_{d_2}\left(v_{b_2} - v_{B_2}\right) + \frac{1}{2}\left[Y_{c_2}\left(v_{a_2} - v_{A_2}\right) + Y_{c_4}\left(v_{a_4} - v_{A_4}\right)\right]\right\}$$

3. RESULTS AND DISCUSSION

An example of a laminated cylindrical shell with clamped ends subjected to simultaneous axial compression and external pressure, shown in Fig.1-ia, is presented here. The loading case of axial compression combined with internal pressure will also be considered. The delamination is located symmetrically with respect to both ends of the shell and it spans the entire circumference. The dimensions of the shell employed throughout this study are such that L/r=5 and r/t=30. This is similar to the geometry employed in Ref. [3], where the structure was subject to pure axial compression. The lamina engineering constants for the selected materials are shown in Table 1. In order to examine the effect of the stacking sequence on the buckling of delaminated cylinders, two different stacking sequences $[0/90/0]_{10T}$, $[0_2/90/\pm 45/\mu 45/90/0_2]_{2T}$,

respectively, are chosen for the analysis. Throughout this study the external pressure is assumed to be positive and the internal pressure is assumed to be negative.

Table 1 Lamina engineering constants for the selected materials

Material No.	E_L/E_T	ν_{LT}	G_{LT}/E_T	G_{TT}/G_{LT}	E_T(GPa)
Graphite-epoxy	40	0.25	0.5	1.0	5.17
Kevlar-epoxy	15.6	0.35	0.56	1.0	5.5
Boron-epoxy	11.11	0.21	0.24	1.0	18.61

First, the eigenvalue analysis was carried out to determine the interaction buckling curve of the intact cylinder, with the stacking sequence of $[0/90/0]_{10T}$. The analysis was carried out for three different materials; graphite-epoxy, kevlar-epoxy and boron-epoxy. Fig. 3 shows the interaction buckling curves, relating pressure (P/P_c) and axial compressive load(R/R_c), through a range of values of P, from buckling under external pressure($P=P_c$) to internal pressure ($P=-P_c$), for the selected materials. R_c and P_c are the critical axial compressive load and critical external pressure of an intact cylinder under axial compressive load alone and external pressure alone, respectively.

The results show that for the selected materials, the trends of the variation of the interaction curves are similar. Therefore, for the intact cylinder, the material properties do not have a great influence on the variation of the interaction buckling curve. Next, the effect of the stacking sequence of the laminate on the shape of the interaction buckling curve is investigated. Fig.3 also shows the interaction buckling curve for the stacking sequence of $\left[0_2/90/\pm 45/-+45/90/0_2\right]_{2T}$ with the graphite-epoxy material properties. For the sake of brevity, the results for the kevlar-epoxy and boron epoxy cylinders with the aforementioned stacking sequence are obtained but are not presented. However, they have similar trends as the interaction curve of the graphite-epoxy. By comparing the interaction buckling curves of the graphite-epoxy cylinder with the two different stacking sequences, it can be observed that the shape of the interaction buckling curve is mainly influenced by the stacking sequence. The difference between the interaction curves is less evident when the cylinder

is subject to internal pressure and more apparent when the cylinder is subject to high level of external pressure.

Figs. 4-a to 4-c show the first buckling mode of an intact graphite-epoxy cylinder with the stacking sequence of $[0/90/0]_{10T}$, subject to the axial compressive load alone, the external pressure load alone and the combined axial compression with pressure, respectively.

Next, the eigenvalue buckling analysis was performed on a delaminated cylinder under the combined axial compression and pressure to determine its corresponding critical values. As explained in section 2 of this paper, for each combined loading case, a live pressure load (P_{cr}) was initially applied to the shell, and then an axial compressive load was applied to the pressurized shell to determine its critical value (R_{cr}). Using ABAQUS it is also possible to apply an axial compressive load in the first step and to determine the critical buckling pressure in the following step. The results will be almost identical.

The results are computed for different delamination sizes, with two different delamination thicknesses, h=0.3 and 0.5, respectively. The delamination length ($\bar{a}$) varies as $0.02 \pi \bar{a} \pi 0.42$. Fig. 5-i shows the variation of the critical axial compression (R_{cr}/R_c) with respect to the delamination length ($\bar{a}$), at different pressure levels, when h=0.5. The cylinder is a laminated graphite-epoxy with the stacking sequence of $[0/90/0]_{10T}$. The pressure level varies from $-1.24P_c$ to $0.93P_c$. A similar set of results for the delamination thickness of h=0.3 can be found in Fig.5-ii. The results for the axial compressive load alone (P=0.), obtained from Ref. [3], are also presented in Figs. 5-i and 5-ii. The following observations have been made from this study.

The internal pressure increases the critical axial load and onset of the buckling mode. For a very small delamination length ($\bar{a} < 0.01$), the presence of delamination does not appreciably alter the critical load of a perfect geometry under the same loading condition. For $P<0.31P_c$, the trends of the variation of the buckling curves with respect to the delamination length ($\bar{a}$) are similar to the buckling curves of the delaminated cylinder under axial compressive load alone(P=0.). For P>0.31Pc, the critical axial load decreases

dramatically with respect to the increase of the delamination length. However, for P=0.47P_c when $\bar{a} < 0.08$ and h=0.5, the critical axial load has a small rate of change with respect to the increase of the delamination length, and it decreases considerably when $\bar{a} \phi 0.08$. Also for P=0.47P_c, when $\bar{a} < 0.125$ and h=0.3, the critical buckling load declines slightly with respect to the increase of the delamination length and for $\bar{a} > 0.125$, there is a sharp drop in the buckling load. For external pressure levels of P=0.93P_c, 0.78P_c and 0.62P_c when h=0.5, the maximum permissible delamination lengths were below $\bar{a}$ =0.042, 0.167 and 0.25, respectively. For the aforementioned delamination lengths, the values of the critical buckling pressure ,in the absence of the axial compressive load, were 0.94P_c, 0.79P_c and 0.69P_c, respectively. The values of the critical buckling pressure for the delamination lengths of $\bar{a}$ =0.042, 0.167 and 0.25, when h=0.3, were 0.96P_c, 0.84P_c and 0.76Pc, respectively.

Fig.5-iii compares the interaction curves of the delaminated graphite-epoxy cylinder for the external pressure levels of P=0.16P_c, 0.31P_c and 0.47P_c, with two different delamination thicknesses of h=0.3 and 0.5, respectively. The results show that for $\bar{a} < 0.08$, the critical buckling curves for h=0.3 and 0.5 are reasonably close. However, when $\bar{a} > 0.08$, for the same delamination size, the delamination which is located on the mid-surface of the cylindrical shell, creates the lower buckling load. The three-dimensional graphs in Figs. 6-i and 6-ii show the effect of the delamination size and pressure on the critical axial compression of the shell for the delamination thicknesses of h=0.5 and 0.3, respectively.

It has to be mentioned that the results in Refs.[3-4] show that for large delamination areas, especially as the position of delamination moves closer to the free surface of the laminate ($h \leq 0.1$), the critical load is very small. In this case, the critical load is not related to the load-carrying capacity of the system and failure will be due to the delamination growth, which depends on the fracture toughness of the material.

Fig. 7-i shows the interaction buckling curve for the delaminated graphite-epoxy cylindrical shell, relating (P/P_c) and (R/R_c), through a range of values of P from buckling under external pressure ($P=P_c$) to internal pressure ($P=-P_c$). The stacking sequence of the

shell is $[0/90/0]_{10T}$ and delamination thickness is h=0.5. The delamination thickness varies as $0.02 < \bar{a} < 0.42$. The interaction curve of the intact cylinder is also included in Fig.7-i. The results show that, for a very small delamination length ($\bar{a} < 0.01$), the presence of delamination does not appreciably alter the interaction buckling curve of an intact cylinder. For large delamination areas, $\bar{a} > 0.375$, the shape of the interaction curve is almost independent of the increase of the delamination length. For a delamination length of $\bar{a} < 0.25$ when P/Pc<0.47, there is almost a linear variation of R/R_c with respect to P/P_c, with a relatively small rate of change. However, for P/P_c>0.47, the rate of change of R/R_c with respect to P/P_c is very high. Therefore, in this region for a slight increase of the external pressure the critical axial compressive load decreases dramatically. The same behaviour can be observed for $\bar{a} > 0.25$ when P/P_c>0.31.

For the delamination thickness of h=0.3, the same trends of variation of R/R_c, with respect to P/P_c, can be observed. See Fig. 7-ii. Fig. 7-iii compares the interaction curves for the delamination thicknesses of h=0.3 and 0.5, respectively. The presented interaction curves include the delamination lengths of $\bar{a}$ =0.02, 0.125 and 0.416, respectively. It can be seen that, for the same delamination length, the critical load for h=0.5 is lower than the critical load for h=0.3, as explained before. However, the trends of the variation of the curves are similar, regardless of the delamination thickness. It can also be observed that for $\bar{a} \leq 0.02$, the critical buckling curves for h=0.3 and 0.5 are almost identical.

Fig. 8-i compares the interaction buckling curves of the above delaminated cylinder with kevlar-epoxy and graphite-epoxy material properties, for the delamination thickness of h=0.5. The presented results include the delamination lengths of $\bar{a}$ =0.02, 0.125 and 0.416, respectively. It can be seen that the interaction curves for the kevlar-epoxy and boron-epoxy cylinders have similar trends. It can also be observed that, like the intact cylinder, the material properties do not have a great influence on the interaction curves of the delaminated cylinder.

Next, the effect of the stacking sequence on the interaction buckling curve of a delaminated cylinder has been investigated. Fig. 8-ii compares the interaction curves of the graphite-

epoxy with two different stacking sequences, $[0_2/90/\pm 45/-+45/90/0_2]_{2T}$ and $[0/90/0]_{10T}$, respectively . For the sake of brevity, the presented results only include the delamination lengths of $\bar{a}$ =0.02, 0.125 and 0.416, respectively. It can be observed that the stacking sequence has a great influence on the interaction curve of the delaminated cylinder.

Figs 9-i and 9-ii show the first buckling mode of a delaminated graphite-epoxy cylinder with a delmination length of $\bar{a}$ =0.125, under different combinations of axial compression and external pressure, for the delamination thicknesses of h=0.5 and h=0.3, respectively. Obviously, the effect of the delamination on the buckling mode is clearly apparent. It can be seen that for higher values of the external pressure and lower values of the axial compressive load, the buckling is mostly in the global mode. On the other hand, for lower levels of external pressure and higher values of axial compressive load the buckling mode tends to be mainly in the local mode. The reduction of the external pressure will obviously result in the increase of the axial buckling load and therefore, the buckling mode tends to be mostly in the local mode. More details on the buckling modes of the cylindrical shells subject to the pure external pressure or the pure axial compression, can be found in Refs. [3] and [4], respectively.

Next, the postbuckling analysis was performed on a graphite-epoxy delaminated cylinder for the stacking sequence of $[0/90/0]_{10T}$, delamination thickness of h=0.5, and with three different delamination lengths of $\bar{a}$ =0.042, 0.08, 0.125, respectively. The external pressure was assumed to be 0.47Pc. For the postbuckling analysis, the external pressure was applied as a live load in the first step ,and in the next step, the axial compressive load was set to increase up to 1.2 times the critical axial compressive load of a perfect cylinder subjected to axial compressive load alone. Fig. 10 shows the load-shortening response (R/R_c vs U_x/t) of the cylinder subject to the combined loading. U_x is the axial displacement of the cylinder. The effect of delamination length on the postbuckling response is clearly evident. It can be seen that as the delamination length increases, the load capacity drops sharply. This response also shows a dramatic loss of strength after the peak load.

Fig.11 shows the SERR distribution along the crack front of the cylinder with the delamination length of $\bar{a}$ =0.125 and the external pressure of P=0.47P_c, for the different values of the axial compressive load. Obviously the higher the axial compressive load is the higher the SERR along the crack front is. It can be observed that SERR has an almost sinusoidal distribution along the crack front. The numerically negative SERR values express no tendency to grow in the corresponding region. The zero value of SERR indicates that the crack is completely arrested at the corresponding point. It can also be observed that the points with zero values of SERR do not shift with the increase of the axial compressive load.

To investigate the effect of delamination length and external pressure on the SERR distribution along the crack front, the SERR results of six delaminated cylinders under the combined loading are presented. See Fig. 12. All six delaminated cylinders are subject to the same compressive axial load. Three of the delaminated cylinders have the delamination length of $\bar{a}$ =0.125 and are subjected to the external pressure levels of P=0., 0.16P_c, 0.31P_c, respectively. The other three delaminated cylinders have the delamination lengths of $\bar{a}$ =0.042, 0.08, 0.125, respectively, and are under the external pressure of 0.47P_c. The results show that with the increase of the delamination length, the SERR changes dramatically. It can also be seen that the points on the crack front with zero values of SERR, displace with the increase of the delamination length. On the other hand, for the same delamination length, the increase of pressure level will also result to the increase of the SERR distribution along the crack front, as expected.

The variations of the total SERR with normalized axial compressive load, for the six delaminated cylinders mentioned above, are shown in Fig.13. The presented results in Fig. 12 correspond to the axial compressive load of R=0.625R_c, which is annotated in Fig. 13. Fig.13 shows that for a small delamination length of the cylindrical shell subject to external pressure, the critical axial load can be significantly greater than the critical buckling load of the perfect cylinder subject to the same loading conditions. For larger delamination areas, the evolution of the displacements produced by the applied load is very smooth and does not reflect the early local instabilities in the structure. When the global instability

develops, the displacements dramatically increase with the increase of the applied axial compressive load, indicating the complete loss of load-carrying capacity of the structure. It can also be observed that the higher external pressure advances the delamination growth, therefore, with a slight increase of the external pressure, especially for larger delamination areas, the total SERR changes drastically.

The number of shell elements, designated S8R in ABAQUS [44], which were used for the modelling of the cylindrical shells throughout this study, vary between 2500 and 4600. The lowest size of the delamination length considered in this study was $\bar{a}$ =0.01. The analysis of cylinders with lower delamination areas was at the expense of the increase in the computational time and space. However, using the present method, the double-layer of shell elements is only used in the delaminated region. On the other hand, as mentioned earlier for very small delamination areas, regardless of the delamination thickness, the presence of delamination does not appreciably alter the critical load of a perfect geometry under the same loading condition.

4. CONCLUDING REMARKS

Despite their advantages, composites suffer from layer separation or delamination which leads to loss of integrity and most likely to premature failure. The use of three-dimensional finite elements for predicting the delamination buckling of these structures is computationally expensive. Here the combined single-layer and double-layer of shell elements are employed to study the delamination buckling and postbuckling of composite laminated shells subjected to simultaneous loading of axial compression and external pressure. The present method provides an excellent framework for the buckling and postbuckling of delaminated plate and shell structures. It gives accurate results with simplicity of computer modelling, which requires relatively lower computer time and space.

This study continues the previous work done by the author on the buckling and postbuckling analysis of delaminated cylindrical shells under axial compression and external pressure, applied individually. The results show that for very small delamination areas, the presence of delamination does not appreciably alter the critical load of a perfect geometry under the same loading condition. The delamination located on the shell's mid-surface creates a lower critical buckling load. However, for larger delamination areas, as the position of delamination moves near the free surface of the laminate, the critical load is very small. In this case, the critical load is not related to the load-carrying capacity of the structure and failure will be due to the delamination growth, which depends on the fracture toughness of the material.

The interaction buckling curves of intact and delaminated composite cylindrical shells, relating the external pressure and axial compression, were obtained. The results show that the internal pressure increases the critical axial compressive load and delays the start of the buckling mode. On the other hand, external pressure advances the onset of the buckling mode and also delamination growth. For large delamination areas of a laminated cylinder under combined axial compression and external pressure, the SERR changes drastically with a slight increase of the external pressure.

It is also shown that the buckling load was highly influenced by the laminate stacking sequence. Hence, there are stacking sequences that favour delamination growth and others that exhibit high resistance against the crack extension. Therefore, a laminate can be tailored to delamination growth resistance. Hence, the study to determine the influence of stacking sequence on SERR distribution and delamination growth in laminated composite shells under combined loading needs further investigation.

The modelling approach established in this work offers high potential for further development. So far, the material properties were assumed to be linear. However, the structure of the model offers convenient extension to nonlinear behaviour such as friction between the crack surfaces, especially when the cylinder is subject to bending and torsion loads.

5. REFERENCES

1. **Tafreshi, A.,** "Shape optimization of anisotropic structures using the boundary element method", Journal of Strain Analysis, 2003; 3(38): 219-32
2. **Tafreshi, A.**, " Shape design sensitivity analysis of 2D anisotropic structures using the boundary element method", Engineering Analysis with Boundary Elements, 2002; 26: 237-51
3. **Tafreshi, A.,** "Efficient modelling of delamination buckling in composite cylindrical shells under axial compression", Composite structures, 64(2004), 511-520
4. **Tafreshi, A.,** "Delamination buckling and postbuckling in composite cylindrical shells under external pressure", Thin-walled structures, 42/10(2004), 1379-1404
5. **Bolotin, V.V.**, "Delamination in composite structures: its origin, buckling, growth and stability", Composites: Part B, 1996; 27B: 129-45
6. **T.E.Tay**, "Characterization and analysis of delamination fracture in composites: An overview of developments from 1990-2001", Applied Mechanics Review., 2003; 56(1): 1-31
7. **Tafreshi, A. and Oswald T.**, "Global buckling behaviour and local damage propagation in composite plates with embedded delaminations", International Journal of Pressure Vessels and Piping, 80, 1, pp 9-20, 2003
8. **Klug, J., Wu, X.X. and Sun, C.T.,** "Efficient modelling of postbuckling delamination growth in composite laminates using plate elements", AIAA J., 1996; 34(1)1: pp178-84
9. **Chai, H., Babcock, C.A. and Knauss, W.G.,** "One dimensional modelling of failure in laminated plates by delamination buckling", International Journal of Solids and Structures, 1981; 17(11): pp1069-83
10. **Pavier M.J. and Clarke, M.P.,** "A specialised composite plate element for problems of delamination buckling and growth", Composite Structures, 1996; 34: 43-53
11. **Chattopadhyay, A. and Gu, H.,** "New higher order plate theory in modelling delamination buckling of composite laminates", AIAA J, 1994; 32(8): pp1709-1716

12. **Chai, G.B., Banks, W.M. and Rhodes J.**, "Experimental study on the buckling and postbuckling of carbon fibre composite panels with and without interply disbonds", Proceedings of the Institution of Mechanical Engineers: Design in Composite Materials. Mechanical Engineering Publications; 1989, 69-85
13. **Whitcomb, J.D.**, "Three-dimensional analysis of a postbuckled embedded delamination", Journal of Composite Materials, 1989; 23(9); 862-89
14. **Hu, N.,**"Buckling analysis of delaminated laminates with consideration of contact in buckling mode", International Journal For Numerical Methods in Engineering", 1999; 44: 1457-79
15. **Krueger, R. and O'Brien T.K**., "A shell/3D modelling technique for the analysis of delaminated composite laminates", Composites: Part A, 2001; 32: 25-44
16. **Kim, H.S., Chattopadhyay, A. and Ghoshal, A.,** "Characterization of delamination effect on composite laminates using a new generalized layerwise approach", Computers and Structures, 2003; 81: 1555-66
17. **Jaunky, N., Knight N.F. Jr**, "An assessment of shell theories for buckling of circular cylindrical laminated composite panels loaded in axial compression", International Journal of Solids and Structures, 1999; 36: 3799-820
18. **Jaunky, N., Knight, N.F. Jr and Ambur, D.R.,** "Buckling analysis of anisotropic variable-curvature panels and shells", Composite Structures, 1999; 43: 321-29
19. **Chaplin, C.P. and Palazotto, A.N.,** "The collapse of composite cylindrical panels with various thickness using finite element analysis", Computers and Structures, 1996; 60(N5): 797-815
20. **Rezeepazhand, J., Simitses, G.J. and Starnes, J.H. Jr**, "Scale models for laminated cylindrical shells subjected to axial compression", Composite Structures, 1996; 34: 371-9
21. **Tafreshi, A.**,"Numerical analysis of thin torispherical end closures", International Journal of Pressure Vessels and Piping, 1997; 71: 77-88
22. **Tafreshi, A. and Thorpe, T.E.**, "Effects of local departures from nominal dimensions on stresses in thin torispherical end-closures", Journal of Strain Analysis,1996; 31(4): 315-24

23. **Hilburger, M.W. and Starnes Jr, J.H.,** "Effects of imperfections on the buckling response of compression-loaded composite shells", Int. J. of non-linear mechanics, 2002; 37: 623-43

24. **Troshin, V.P.,** "Effect of longitudinal delamination in a laminar cylindrical shell on the critical external pressure", Journal of Composite Materials, 1983; 17(5): 563-7

25. **Simitses, G.J. and Chen, Z.**, "Buckling of delaminated, long, cylindrical panels under pressure", Computers and Structures, 1988; 28(2): 173-84

26. **Simitses, G.J., Chen, Z.Q. and Sallam S.,** "Delamination buckling of cylindrical laminates", Thin-walled Structures, 1991; 11: pp25-41

27. **Sallam, S. and Simitses, G.J.**, "Delamination buckling of cylindrical shells under axial compression", Composite Structures, 1987; 7: 83-101

28. **Short,G.J. Guild, F.J. and Pavier,M.J.** ,"Delaminations in flat and curved composite laminates subjected to compressive load", Composite Structures, 2002; 58: 249-58

29. **Kutlu, Z. and Chang, F.K.**, "Composite panels containing multiple through-the-width delaminations and subjected to compression. Part I: analysis, Composite Structures, 1995; 31: 273-296

30. **Kutlu, Z. and Chang, F.K.**, "Composite panels containing multiple through-the-width delaminations and subjected to compression. Part II: experiments & verification, Composite Structures,1995; 31: 297-314

31. **Naganarayana, B.P., Huang, B.Z. and Atluri S.N.**, "Multidomain modelling and analysis of delaminated stiffened composite shells", AIAA J., 1996 34(9): 1894-904

32. **Gu, H. and Chattopadhyay A.**, "Delamination buckling and postbuckling of composite cylindrical shells", AIAA Journal, 1996, 34(6): 1279-86

33. **Rasheed H.A. and Tassoulas J.L.,** "Delamination growth in long composite tubes under external pressure", International Journal of Fracture, 2001; 108: 1-23

34. **Tafreshi, A.**, "Buckling and post-buckling analysis of composite cylindrical shells with cutouts subjected to internal pressure and axial compression loads" International Journal of Pressure Vessels and Piping, 2002; 79(5): 351-359

35. **Ju-fen Z., Gang, Z., Howson, W.P. and Williams, F.W.,** "Reference surface element modelling of composite plate/shell delamination buckling and postbuckling", Composite Structures, 2003; 61: 255-64

36. **Anastasiadis, J.S., Tabiei, A. and Simitses, G.J**., "Instability of moderately thick, laminated, cylindrical shells under combined axial compression and pressure", Composite structures, 1994; 27:367-78

37. **Shen H.S.,** "Postbuckling of shear deformable cross-ply laminated cylindrical shells under combined external pressure and axial compression", International Journal of Mechanical Sciences, 2001; 43: 2493-523

38. **Adali, S., Verijenko, V.E. and Richter, A.**, "Minimum sensitivity design of laminated shells under axial load and external pressure", Composite structures, 2001; 54: 139-142

39. **Messager, T., Pyrz, M. Gineste, B. and Chauchot, P.**, "Optimal laminations of thin underwater composite cylindrical vessels", Composite Structures, 2002; 58: 529-37

40. **Xue, J. and Fatt, H.**, "Buckling of a non-uniform, long cylindrical shell subjected to external hydrostatic pressure", Engineering Structures, 2002; 24:1027-1034

41. **Featherston, C.A.,** "Imperfection sensitivity of curved panels under combined compression and shear", International journal of non-linear mechanics", 2003; 38: 225-238

42. **Shivakumar, K.N., Tan, P.W. and Newman Jr J.C.,** "A virtual crack closure technique for calculating stress intensity factors for cracked three dimensional bodies", International Journal of Fracture, 1988; 36: 43-50

43. **Raju, I.S. and Shivakumar, K.N.**, " Three-dimensional elastic analysis of a composite double cantilever beam specimen", AIAA Journal, 1988; 26(12): 1493-8

44. **ABAQUS User's Manual**, Version 6.3, Hibbit, Karlson and Sorenson, Inc. 1999-2002

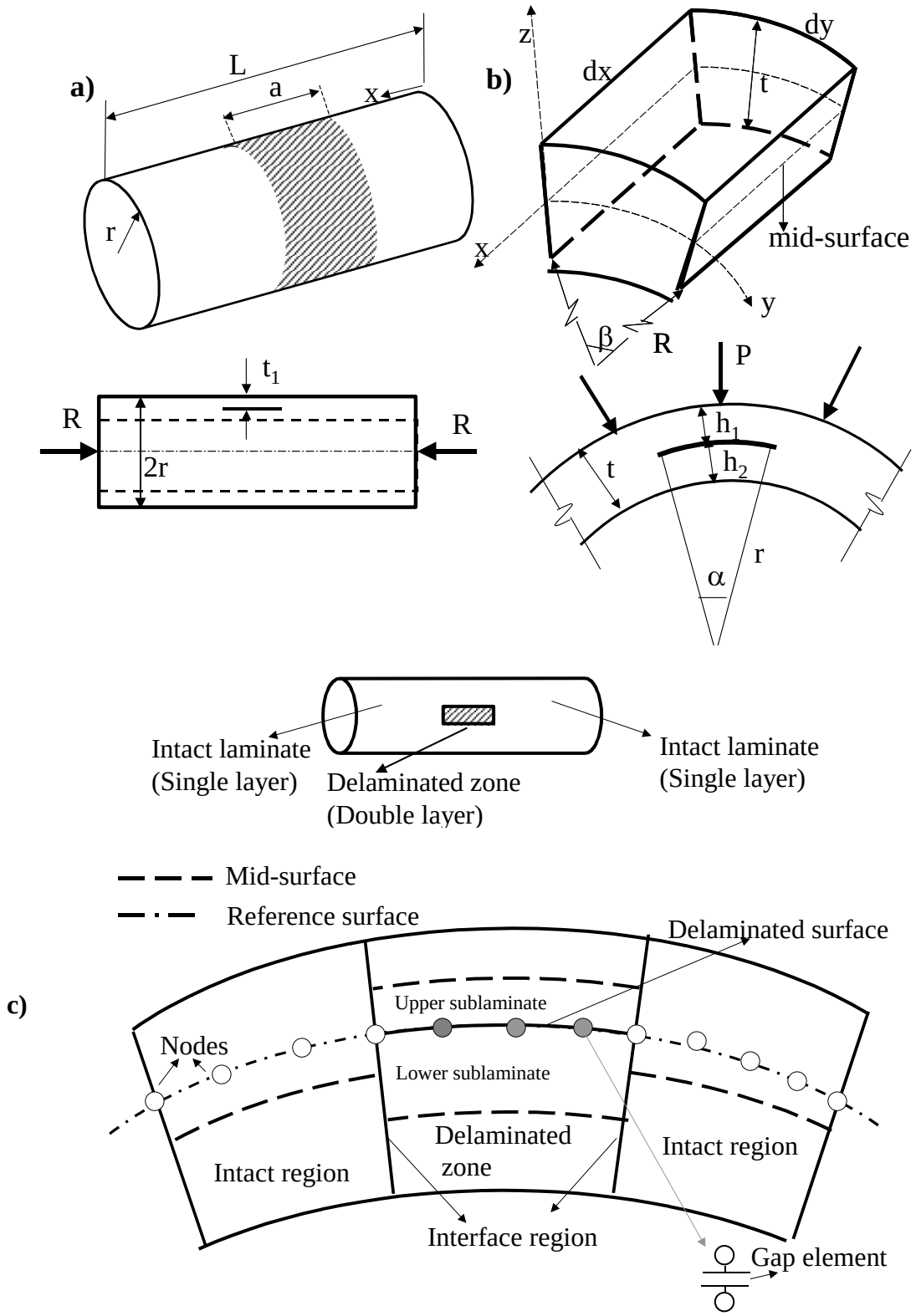

Fig. 1-i a) Geometry of a delaminated cylindrical shell under combined axial compression and external pressure b) a delamination of length(a), extended along its entire circumference b) a cylindrical shell differential element c) close-up view of a typical FE model to be used for a delaminated cylindrical shell where nodes are located on the reference surface offset from the mid-surfaces of the laminate and sublaminates

Fig. 1-ii Effect of delamination length(a/L) (extended along the entire circumference) on the critical axial buckling loads of an isotropic cylindrical shell

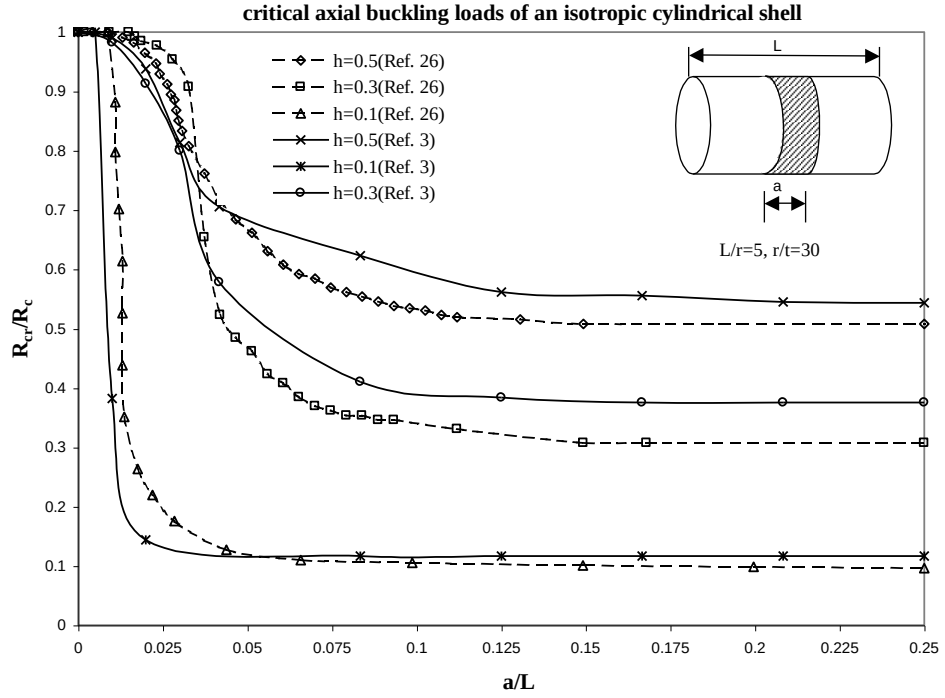

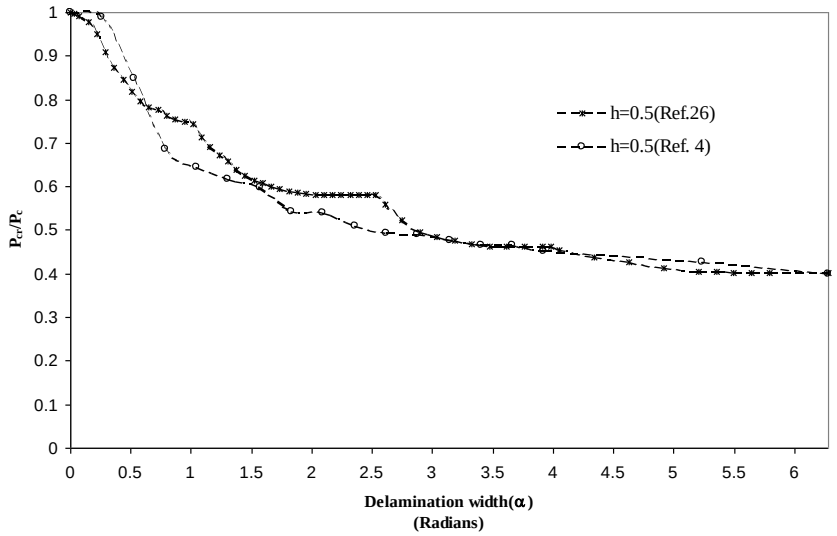

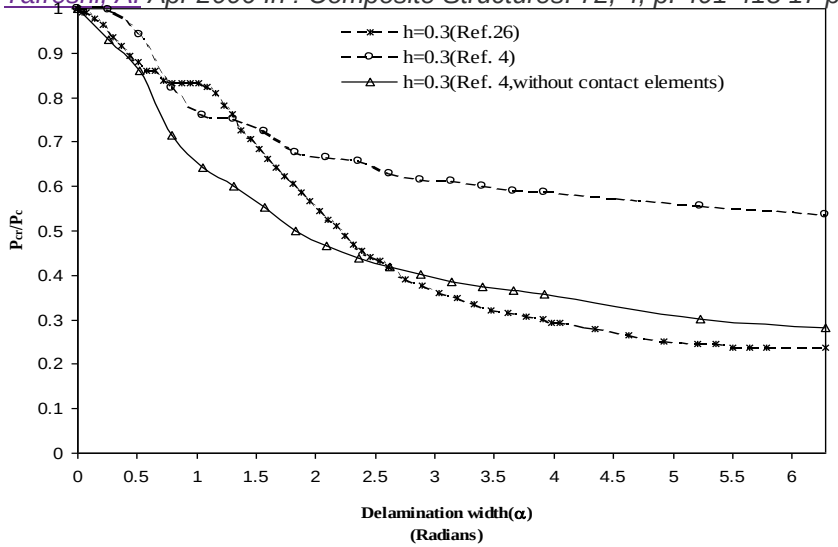

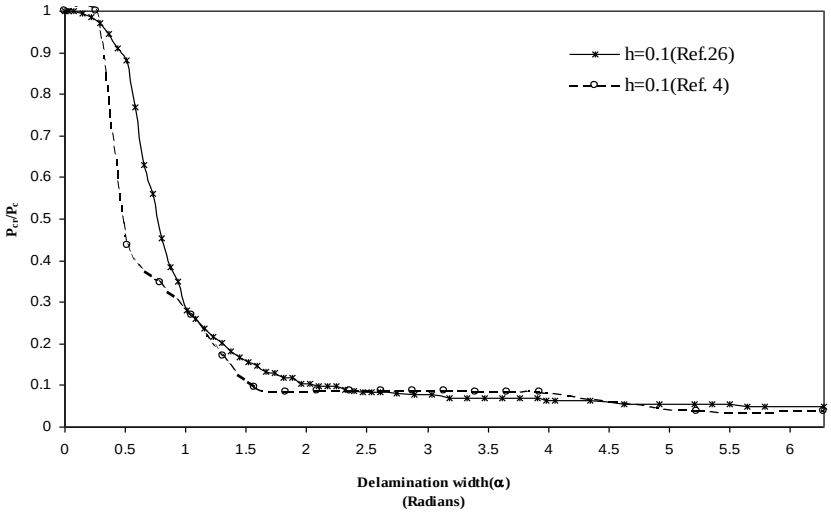

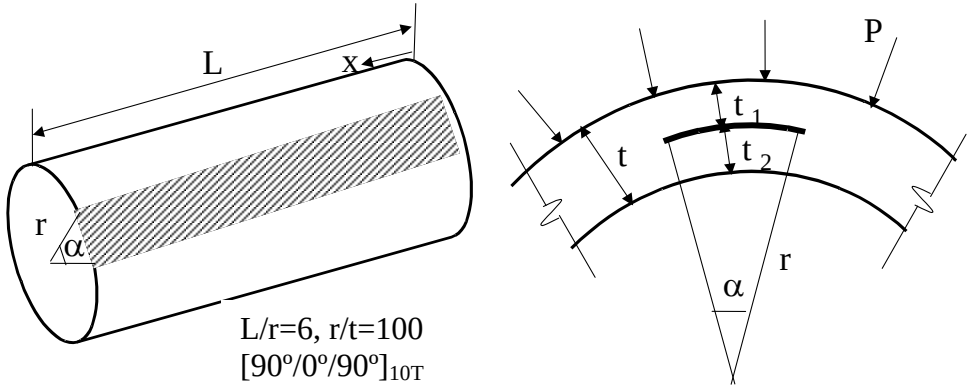

Fig. 1-iii Effect of delamination width(α), extended over the entire length, on the critical buckling external pressure of a graphite-epoxy cylindrical shell
a) h=0.5, b) h=0.3, c) h=0.1

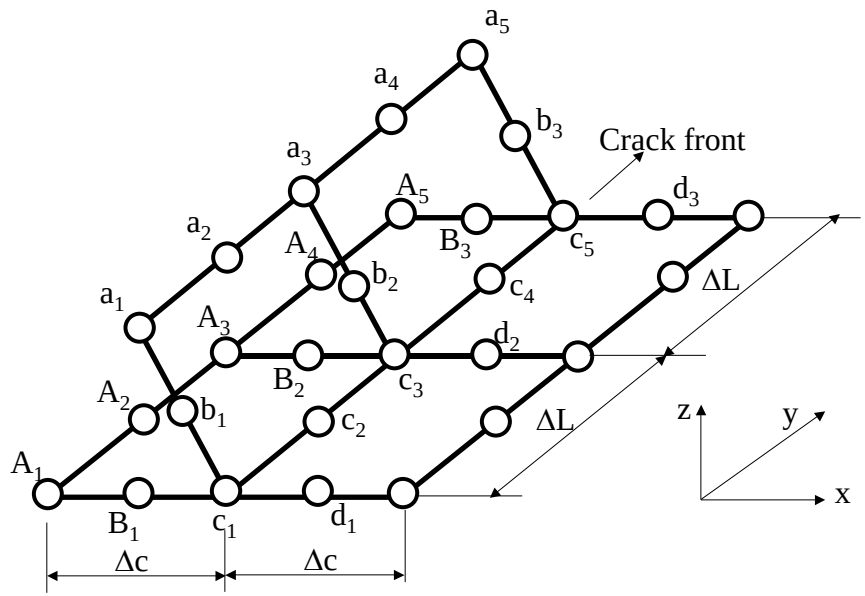

Fig. 2 Schematic of delamination front region

Fig. 3 Interaction buckling curve of an intact cylindrical shell subject to combined axial compression and pressure(L/r=5, r/t=30)

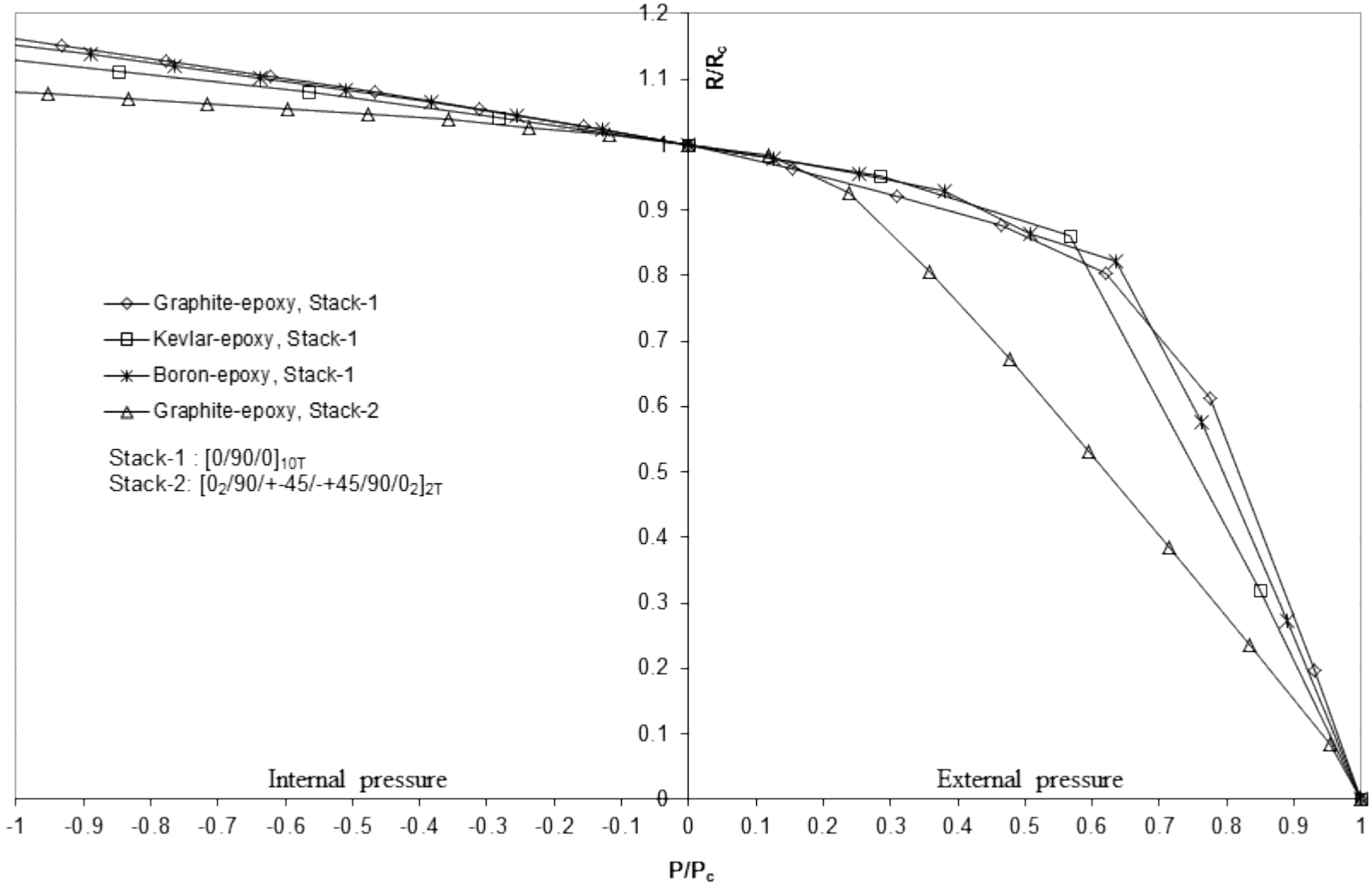

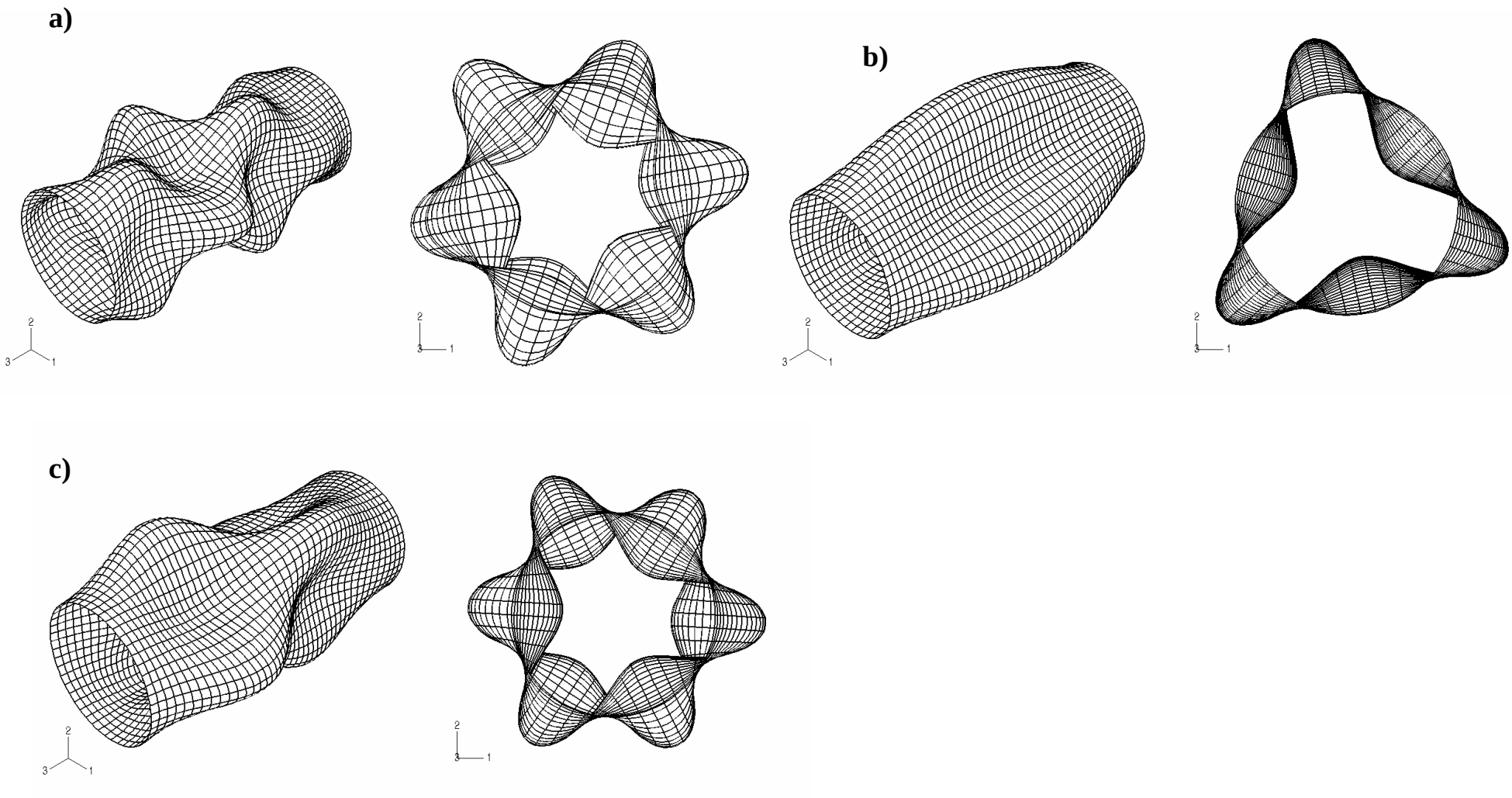

Fig. 4 First buckling mode of an intact graphite-epoxy cylindrical shell(L/r=5, r/t=30) subject to a) Axial compression ($R=R_c$) only, b) External pressure ($P=P_c$) only, c) Axial compression ($R=0.8R_c$) and external pressure($P=0.62P_C$)

Fig. 5-i Effect of delamination length on the critical axial compression(R_{cr}) of a delaminated graphite-epoxy cylindrical shell subject to combined axial compression(R) and pressure(P), L/r=5, r/t=30, h=0.5, $[0/90/0]_{10T}$

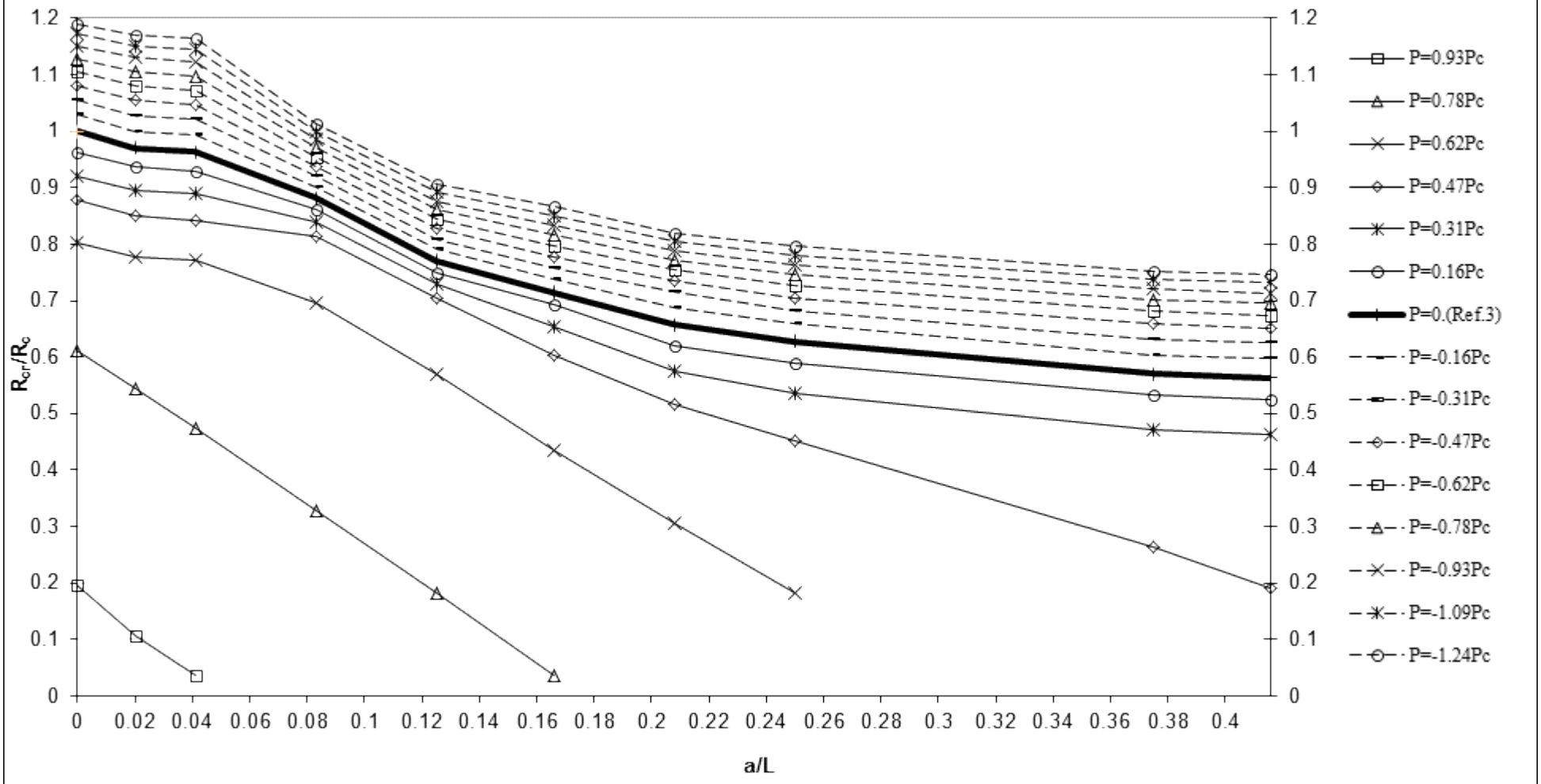

Fig. 5-ii Effect of delamination length on the critical axial compression of a delaminated graphite-epoxy cylindrical shell subject to combined axial compression and pressure, L/r=5, r/t=30, h=0.3, $[0/90/0]_{10T}$

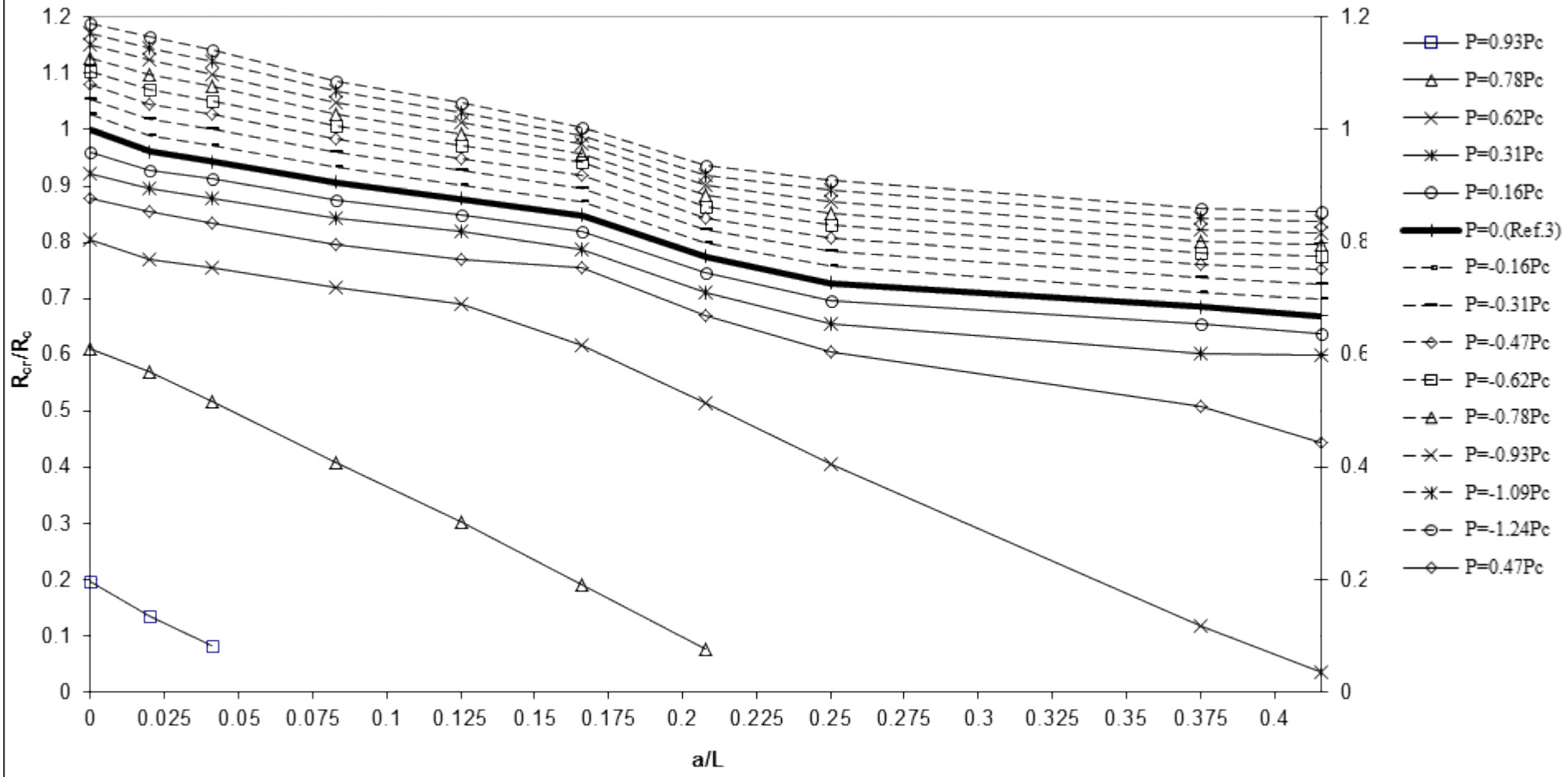

Fig. 5-iii Effect of delamination width, delamination thickness and external pressure on the critical axial compression of a graphite-epoxy cylindrical shell, r/t=30, L/r=5, $[0/90/0]_{10T}$

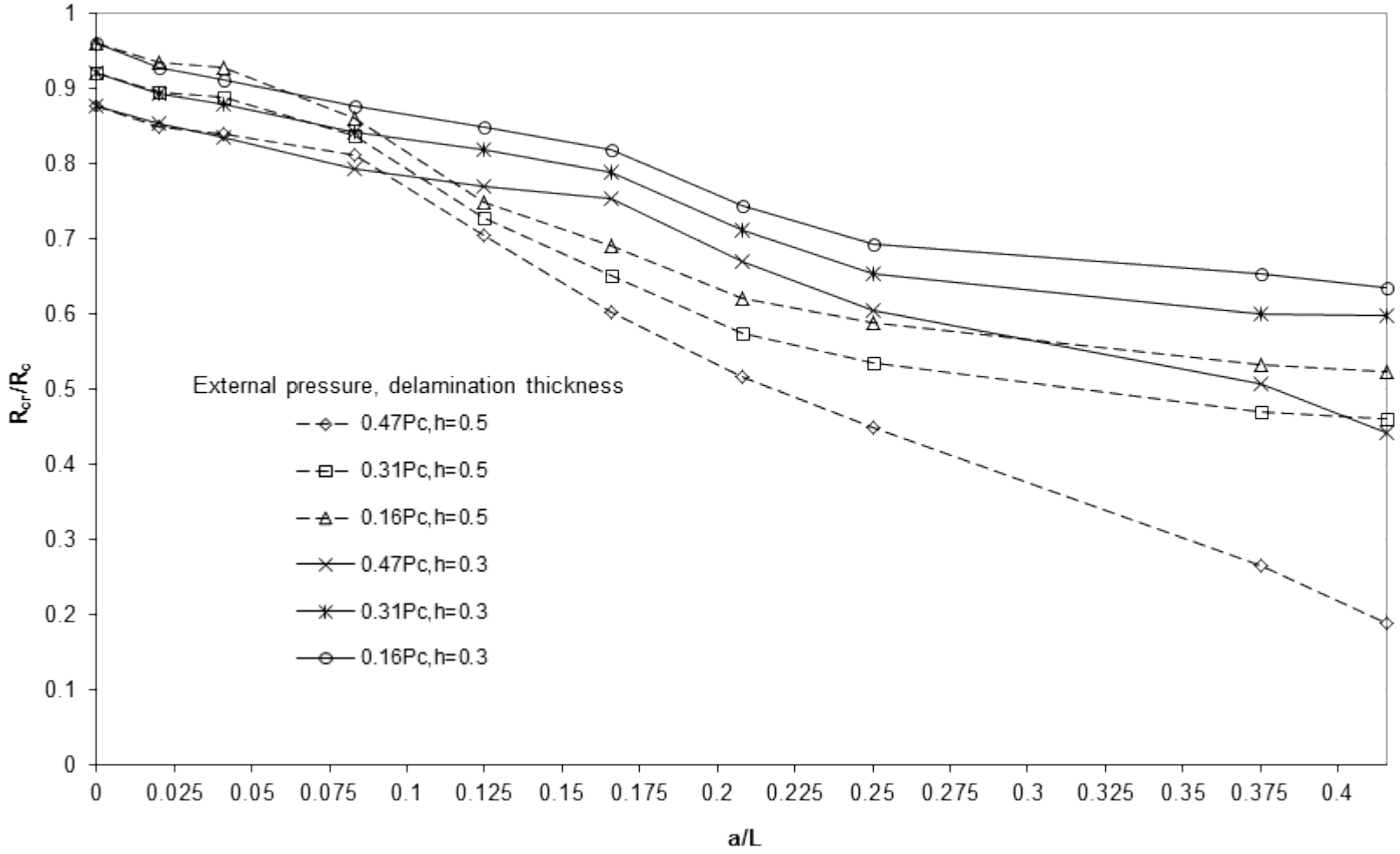

Fig. 6-i Effect of delamination length and pressure on the critical axial compression of a graphite-epoxy cylindrical shell, h=0.5, r/t=30, L/r=5, $[0/90/0]_{10T}$

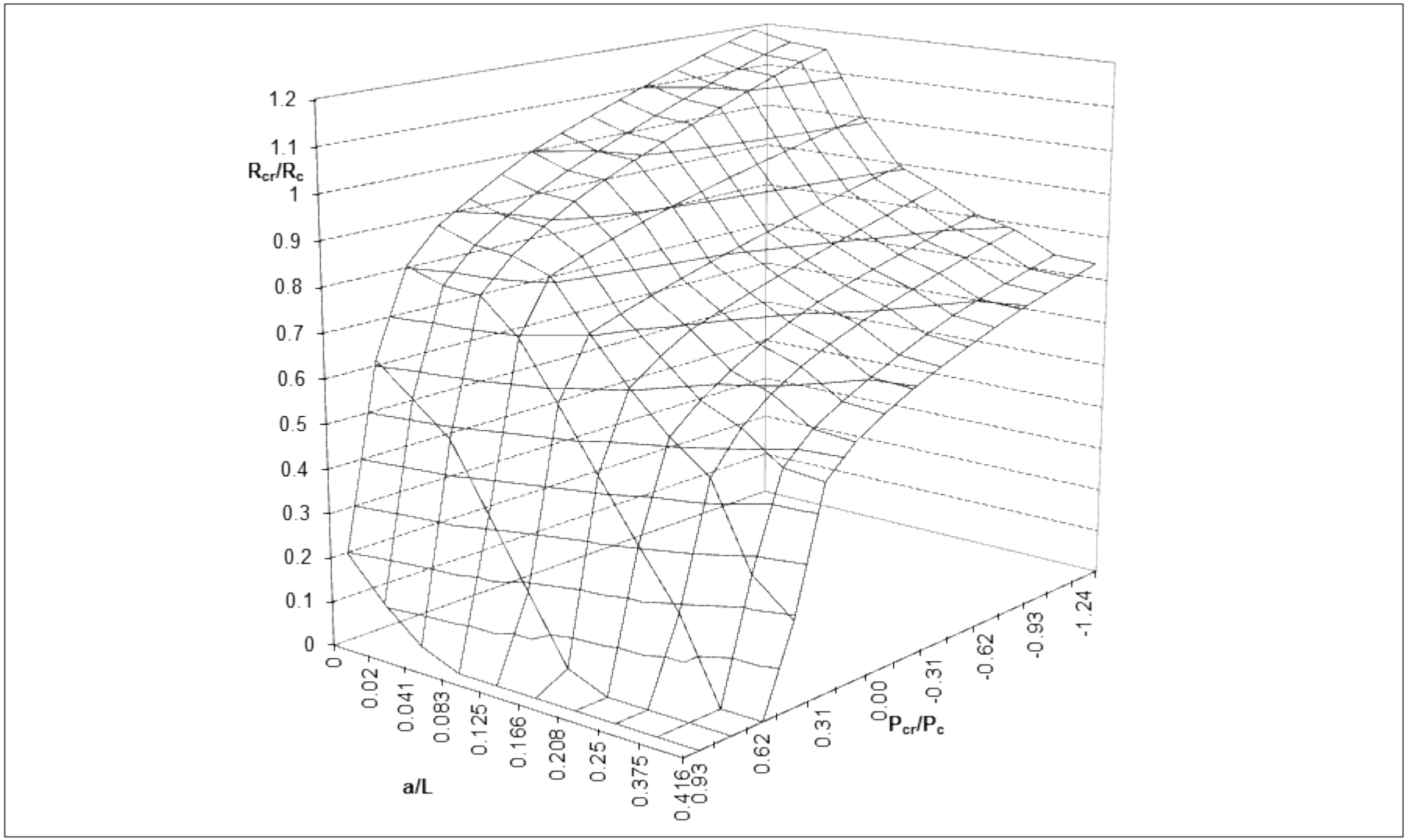

Fig. 6-ii Effect of delamination length and pressure on the critical axial compressive load of a graphite-epoxy cylindrical shell, h=0.3, r/t=30, L/r=5, $[0/90/0]_{10T}$

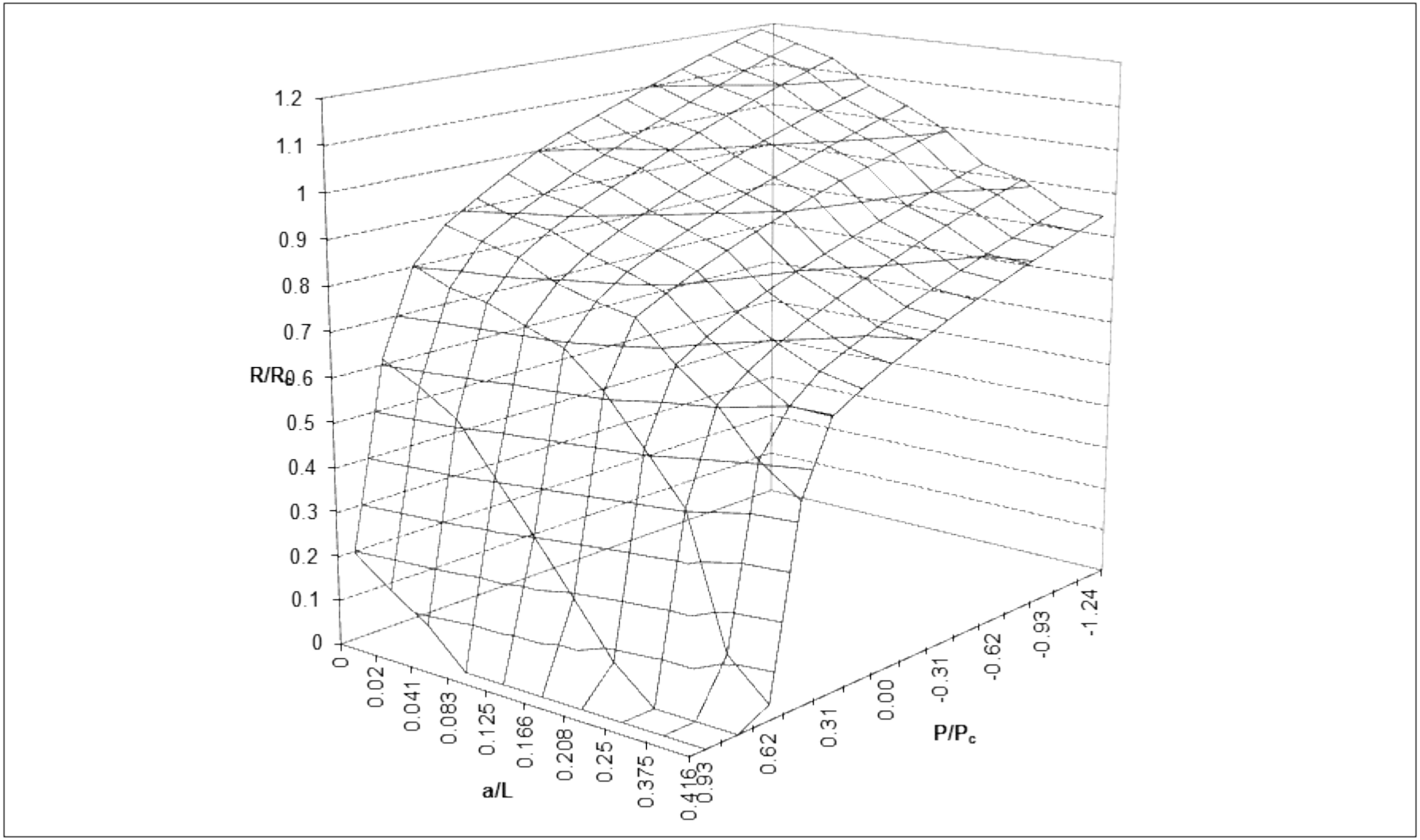

Fig. 7-i Interaction buckling curve for the intact and delaminated graphite-epoxy cylindrical shells, r/t=30, L/r=5, h=0.5, $[0/90/0]_{10T}$

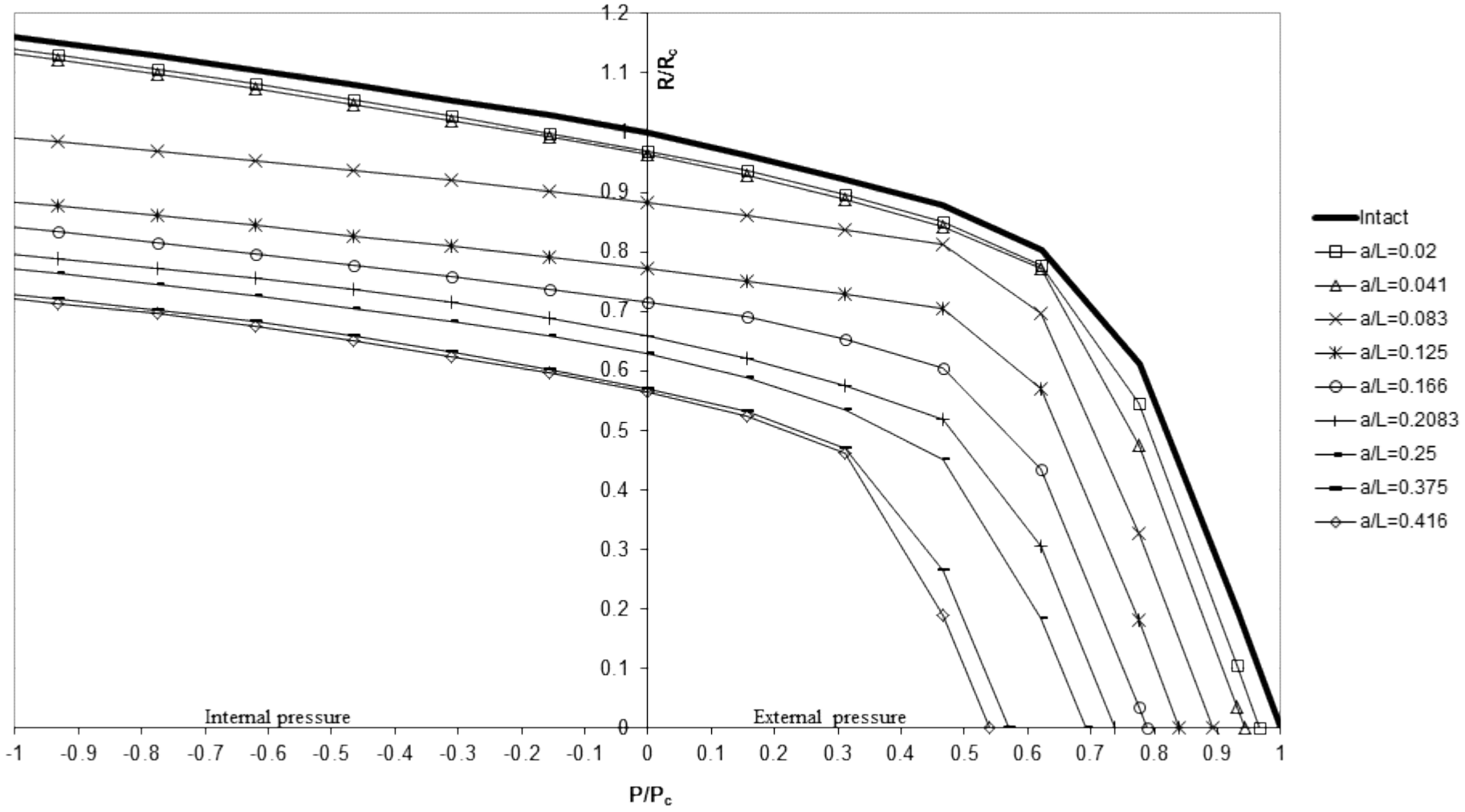

Fig. 7-ii Interaction buckling curve for the intact and delaminated graphite-epoxy cylindrical shells, R/t=30, L/R=5, h=0.3, $[0/90/0]_{10T}$

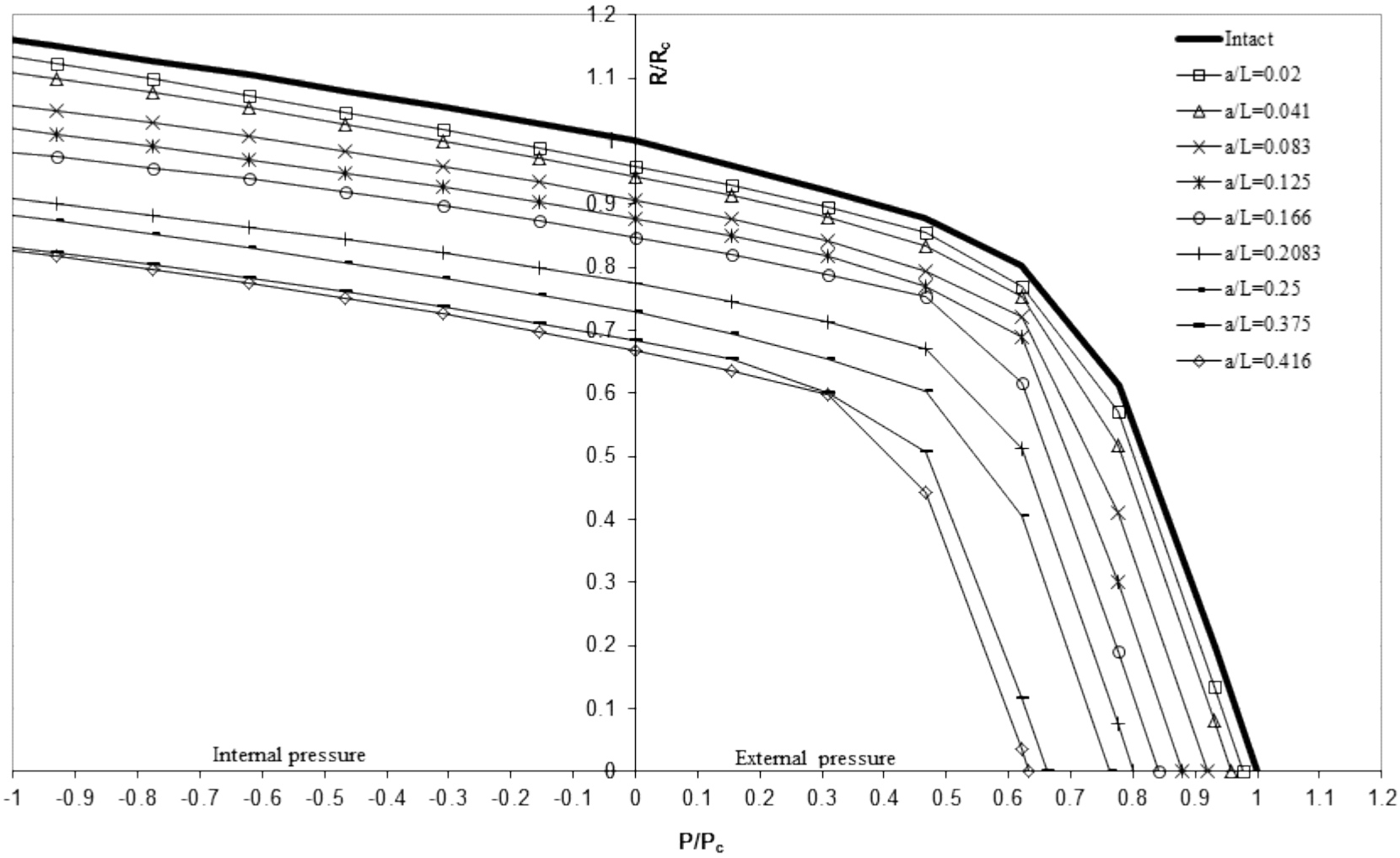

Fig. 7-iii Comparison between the interaction buckling curves of delaminated cylindrical shells with different delamination thicknesses r/t=30, L/r=5, h=0.3 & 0.5, $[0/90/0]_{10T}$

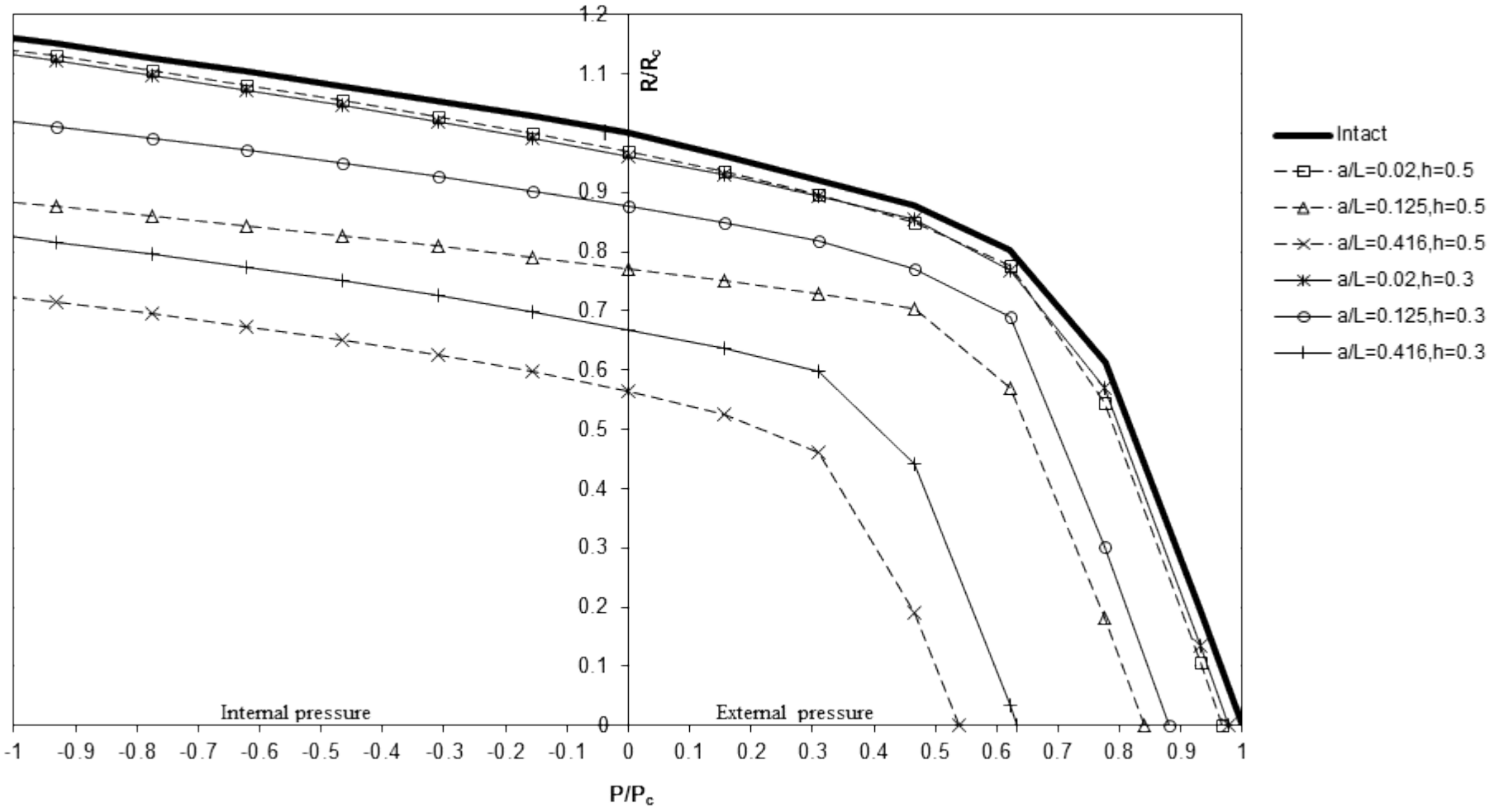

Fig. 8-i Effect of the material properties on the interaction buckling curve of a composite cylindrical shell, r/t=30, h=0.5, L/r=5, $[0/90/0]_{10T}$

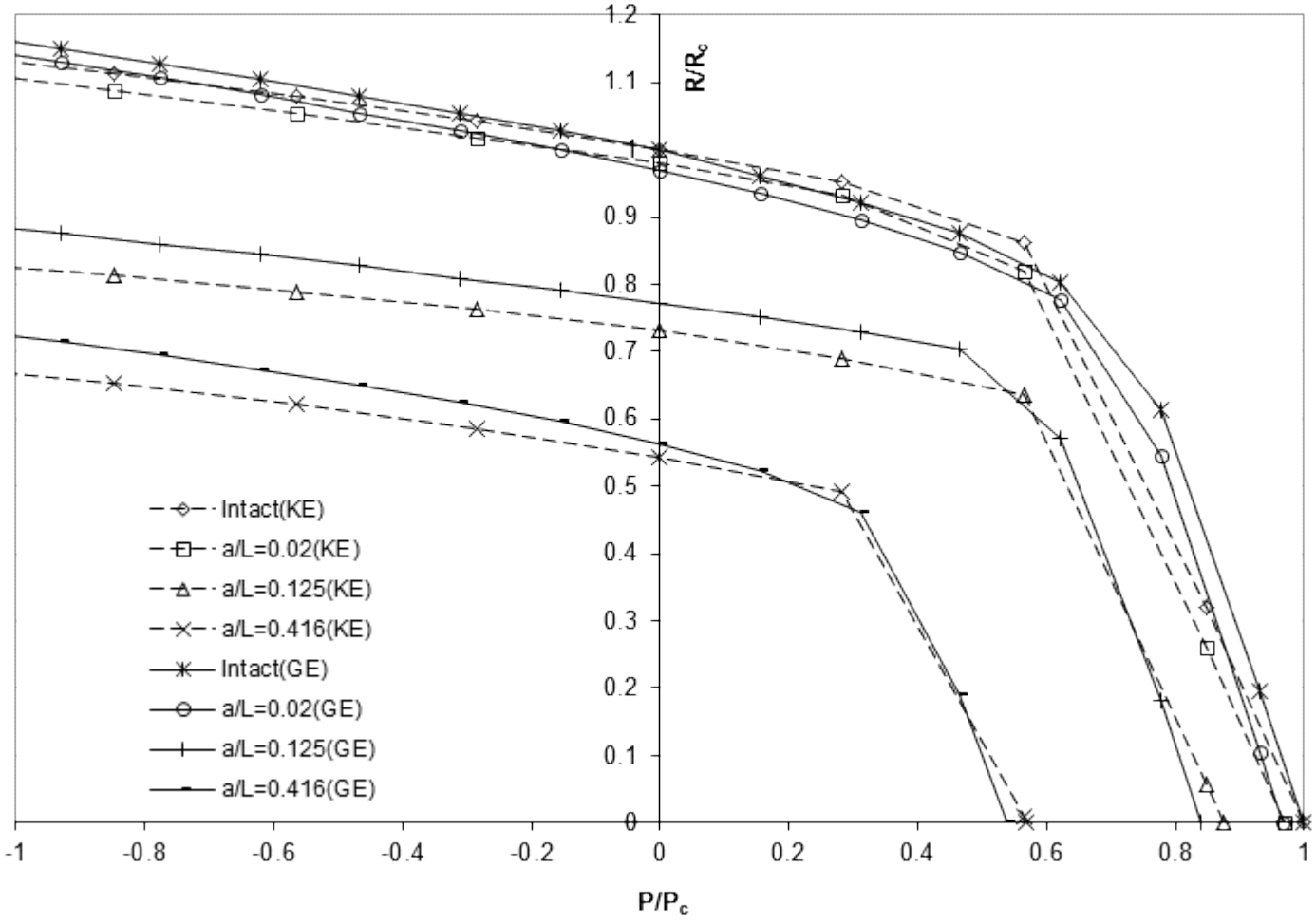

Fig. 8-ii Effect of the stacking sequence on the interaction buckling curve of a graphite-epoxy cylindrical shell, r/t=30, L/r=5, h=0.5

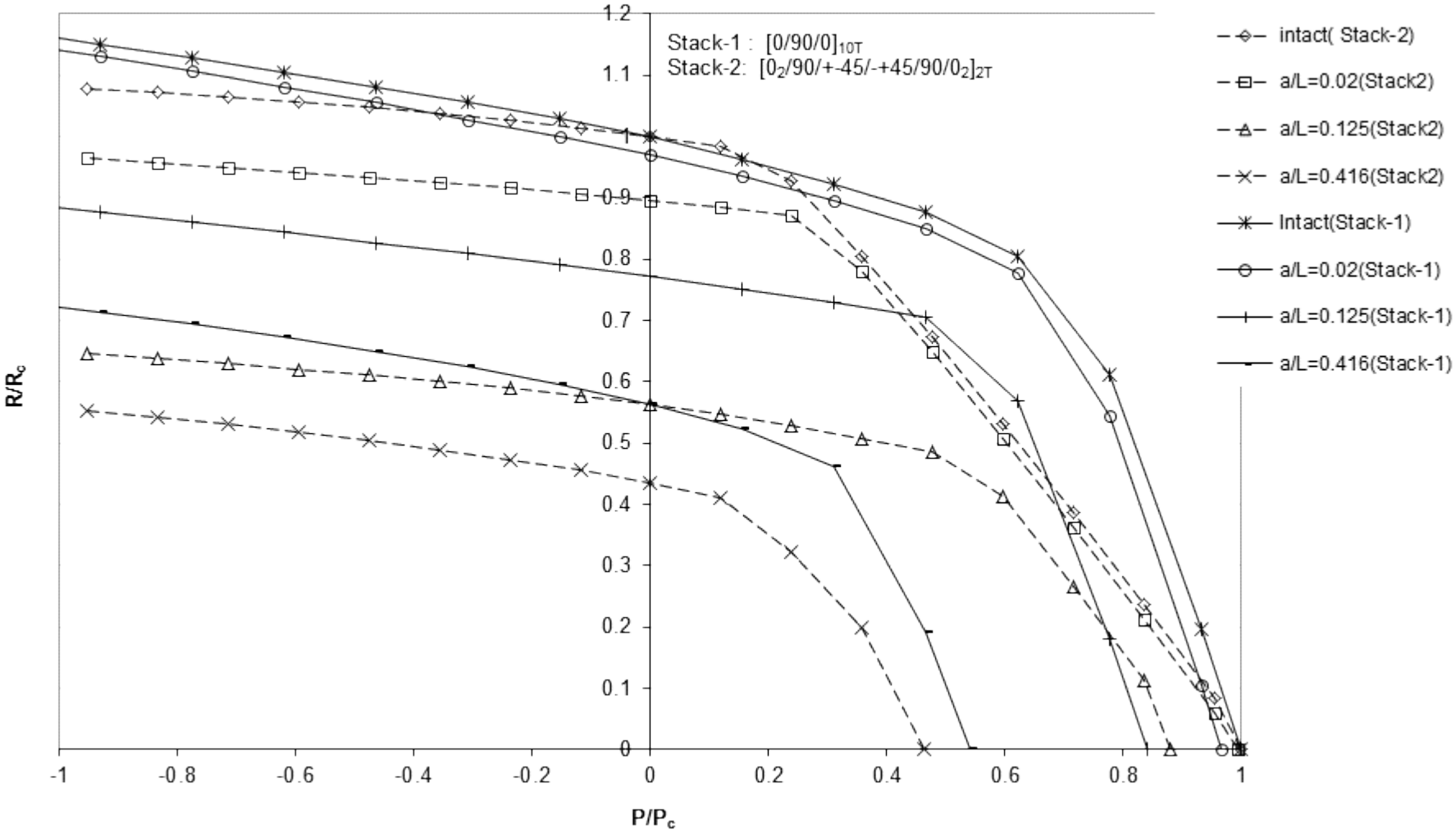

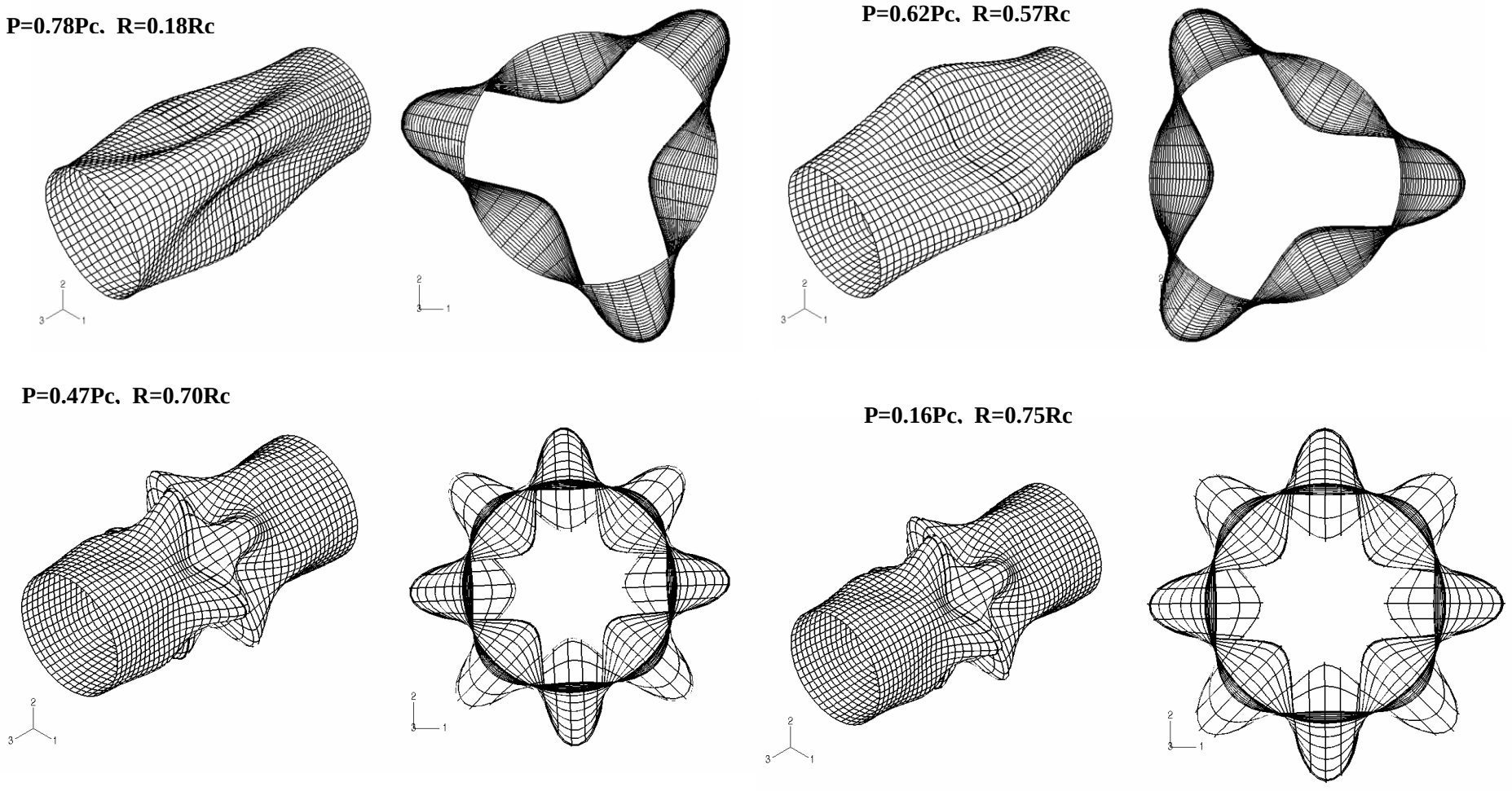

Fig. 9-i The first buckling mode of the graphite-epoxy cylindrical shell with the stacking sequence of $[0/90/0]_{10T}$, delamination thickness of h=0.5 and delamination width of a/L=0.125, under different combinations of axial compression and external pressure

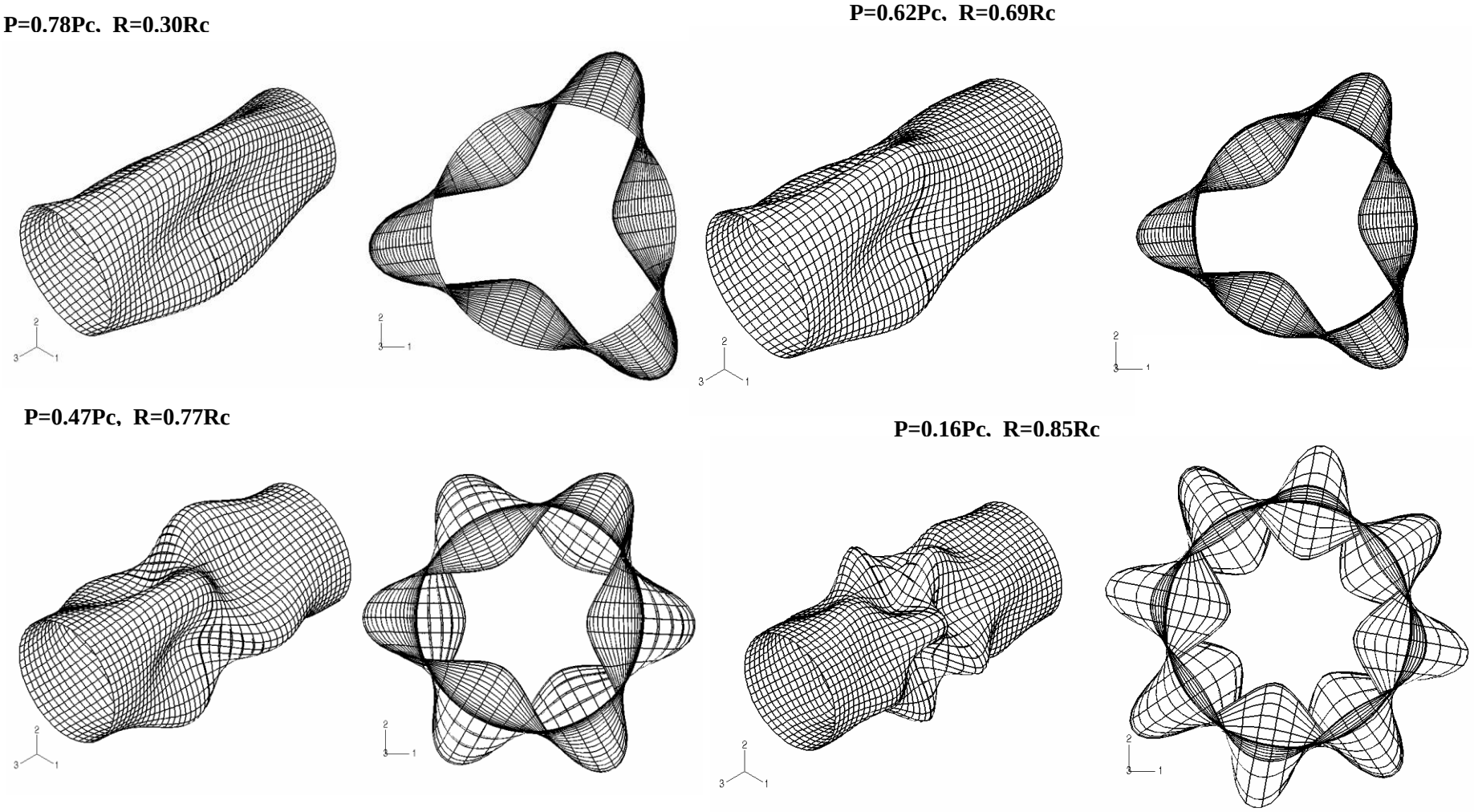

Fig. 9-ii The first buckling mode of the graphite-epoxy cylindrical shell with the stacking sequence of $[0/90/0]_{10T}$, delamination thickness of h=0.3 and delamination width of a/L=0.125, under different combinations of axial compression and external pressure

Fig. 10 Load-shortening response of a graphite-epoxy cylindrical shell under combined axial compression and external pressure, L/r=5, r/t=30, h=0.5, $[0/90/0]_{10T}$

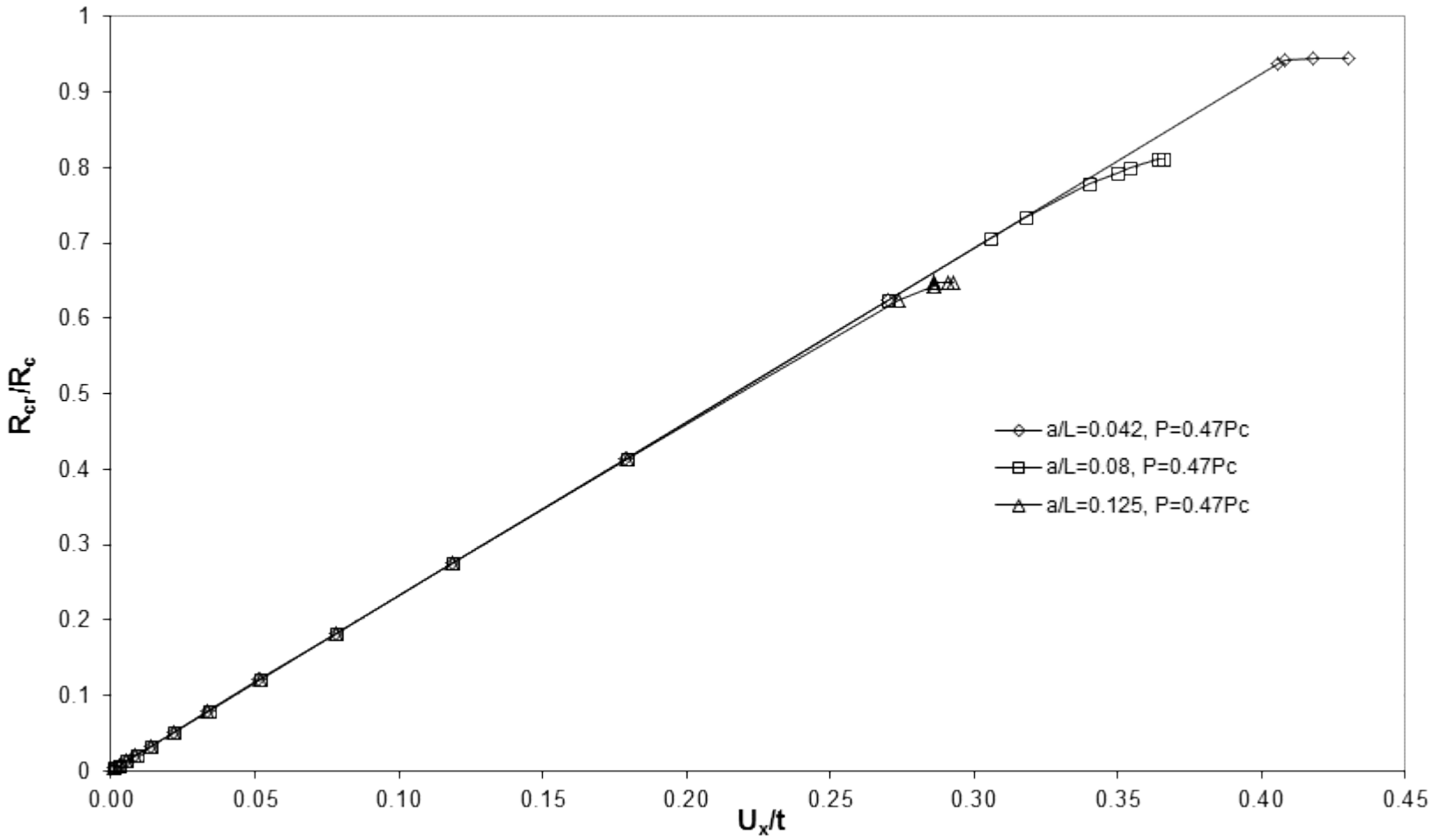

Fig. 11 Strain energy release rate distribution along the crack front for a delaminated graphite epoxy cylindrical shell with delamination length of a/L=0.125, h=0.5, L/r=5, r/t=30, P=0.46P_c

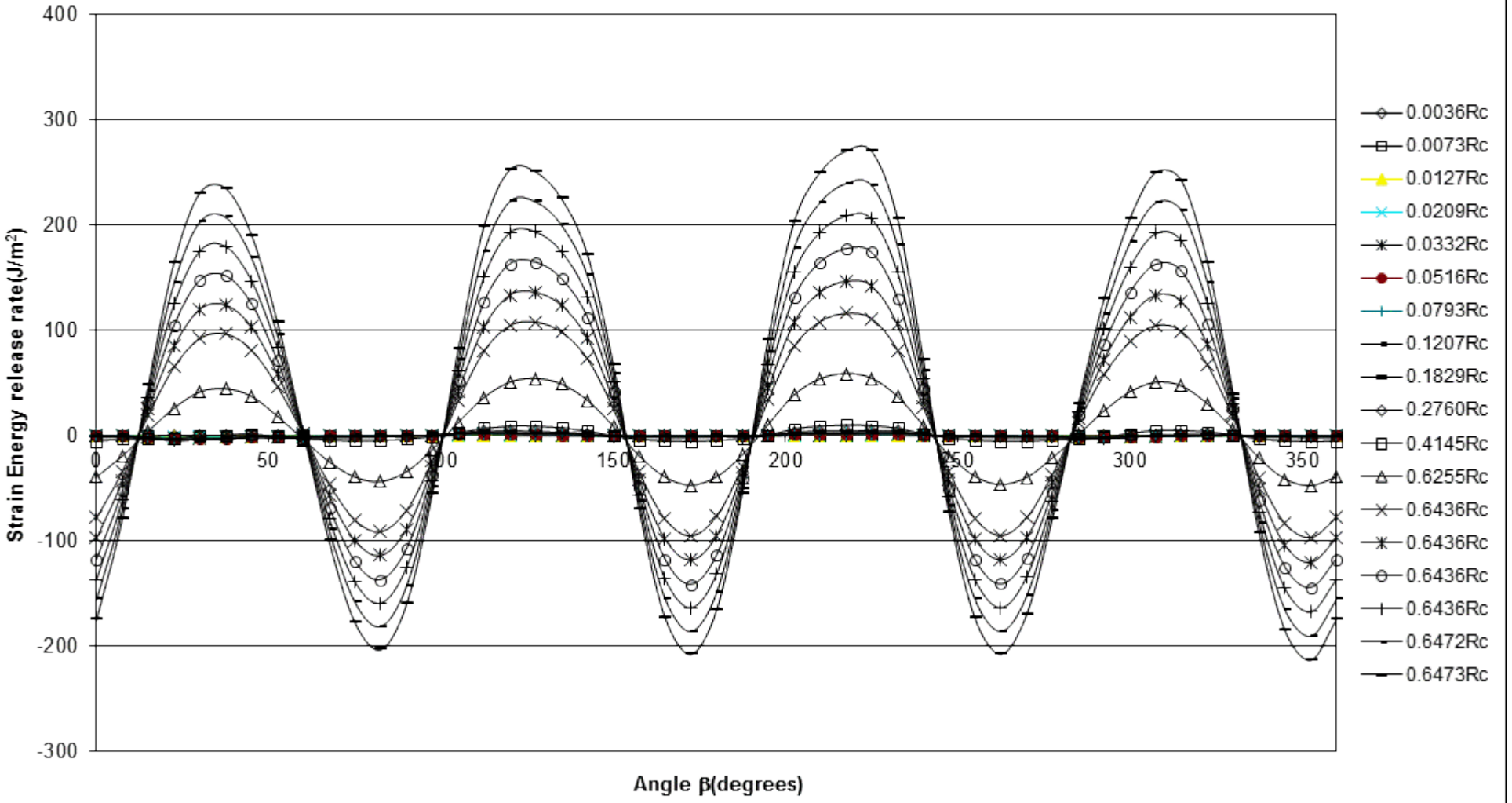

Fig. 12 Strain energy release rate distribution along the crack front of a delaminated graphite-epoxy cylindrical shell under the combined axial compression and external pressure, L/r=5, R/t=30, h=0.5, R=0.625Rc

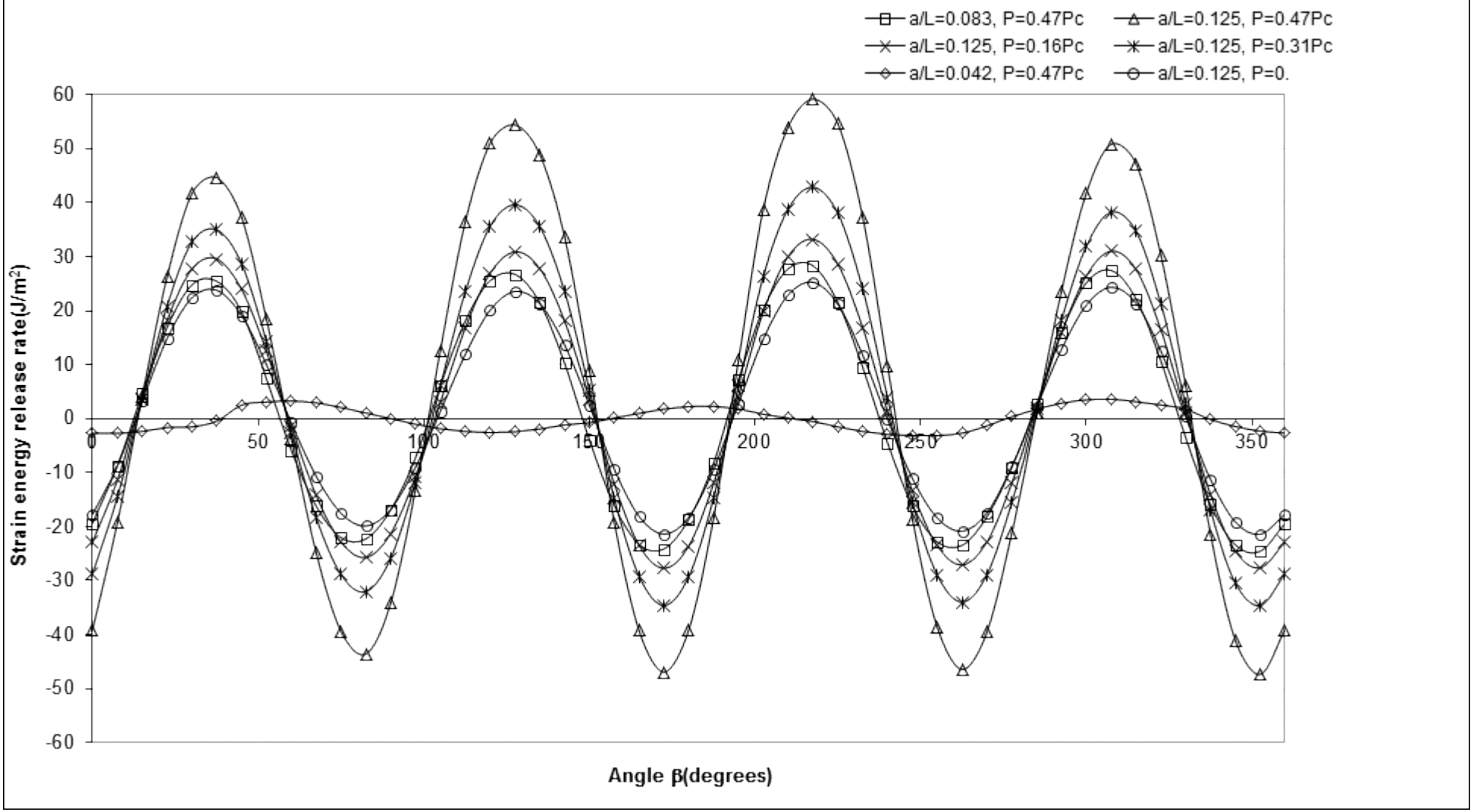

Fig. 13 Total strain energy release rate of a delaminated graphite-epoxy cylindrical shell under the combined axial compression and external pressure, L/r=5, r/t=30, h=0.5, $[0/90/0]_{10T}$